

University of Houston  
Department of Mechanical Engineering  
Houston, Texas 77004

NASA CR-134383

CHARACTERIZATION OF HEAT TRANSFER IN NUTRIENT MATERIALS

by

J. E. Cox    R. B. Bannerot    C. K. Chen    L. C. Witte

Final Report, Part II

Report No. NAS-9-11676-32

31 December 1973

(NASA-CR-134383) CHARACTERIZATION OF HEAT  
TRANSFER IN NUTRIENT MATERIALS, PART 2  
Final Report (Houston Univ.)

N74-30500

Unclas

G3/05 46870

Sponsor: National Aeronautics and Space Administration

Contract: NAS 9-11676

Reproduction in whole or in part is permitted for any  
purpose of the United States Government. Distribution  
of the report is unlimited.

PRICES SUBJECT TO CHANGE

Reproduced by  
NATIONAL TECHNICAL  
INFORMATION SERVICE  
U.S. Department of Commerce  
Springfield, VA. 22151



University of Houston  
Department of Mechanical Engineering  
Houston, Texas 77004

**CHARACTERIZATION OF HEAT TRANSFER IN NUTRIENT MATERIALS**

~~XXXXXXXXXXXXXXXXXXXX~~ Report No. NAS 9-11676-32

31 December 1973

Sponsor: NASA - Johnson Space Center  
Houston, Texas 77058


Contract: NAS 9-11676

Technical Monitor: Dr. N. D. Heidelbaugh (DC-71)  
Foods and Nutrition Branch  
Preventive Medicine Division

Contract Negotiator: Mr. A. M. Cornelius (BC-7)  
R & T Procurement Branch

Approved:

  
\_\_\_\_\_  
L. C. Witte, Co-Director

  
\_\_\_\_\_  
J. E. Cox, Director

## TABLE OF CONTENTS

Nomenclature

### PART II

6.0	Inclusion of Phase Change (Melting) in the Thermal Model ..	1
6.1	The Thermal Model	
6.2	Results	
7.0	Low-Gravity Considerations .....	5
7.1	Liquid/Gas Orientation	
7.2	Low-Gravity Heat Transfer	
7.3	Laboratory Simulation of Reduced Gravity	
8.0	Alternate Model .....	12
8.1	Contact Resistance in Skylab Heater	
8.2	Equivalent Thermal Properties	
8.2.1	Equivalent Conductance due to Radiation	
8.2.2	Radial Equivalent Conductance	
8.2.3	Wall Equivalent Conductance	
8.2.4	Equivalent Heat Capacity	
8.3	A Constant Wall-Temperature Model	
8.3.1	The Case for the Constant Wall-Temperature Model	
8.3.2	Initial Results	
8.3.3	Corrected Results	
8.3.3.1	Correction for Maximum Wall Heat Flux	
8.3.3.2	Correction for Reduced Volume in Model	
8.3.3.3	Results	
9.0	Optimization .....	31
9.1	Effect of Thermophysical Properties	
9.2	Effect of Heater Power Level	
9.3	Effect of Initial Temperature	
9.4	Effect of Container Size	
9.5	Effect of Control Temperatures	
9.6	Discussion	

References

## Nomenclature

a	acceleration
A	area
Bo	Bond number, eqn (7-2)
c	specific heat
$E_b$	blackbody emissive power, eqn (8-2)
F	configuration factor, eqn (8-1)
Fr	Froude number, eqn (7-4)
g	acceleration of gravity
$g_0$	standard acceleration of gravity
G	irradiation, eqn (8-2)
Gr	Grashof number
$h_{if}$	latent heat of fusion
J	radiosity, eqn (8-1)
k	thermal conductivity
$k_e$	effective thermal conductivity
L	can height or characteristic length (Section 7)
Nu	Nusselt number
Pr	Prandtl number
q	heat transfer rate
Q	heat transfer
$q''$	heat flux
$q_0$	wall heater flux

$q_{\text{net}}$  net heat transfer rate into a node, eqn (6-1).  
 $q_{\text{in}}$  rate of heat transfer into a node, eqn (6-1)  
 $q_{\text{out}}$  rate of heat transfer out of a node, eqn (6-1)  
 $r$  radial coordinate  
 $R$  can radius  
 $Ra$  Rayleigh number, eqn (7-5)  
 $Ra^*$  modified Rayleigh number, eqn (7-6)  
 $t$  time  
 $t_w$  can wall thickness  
 $T$  temperature  
 $\bar{T}$  average food temperature  
 $\hat{T}$  linearization mean temperature, eqn (8-11)  
 $T_b$  bulk fluid temperature  
 $T_c$  cold-spot temperature  
 $T_i$  initial food temperature  
 $T_{\text{off}}$  heater deactivation temperature (cut-off)  
 $T_{\text{on}}$  heater activation temperature (cut-on)  
 $V$  volume  
 $\bar{V}$  velocity  
 $w$  thickness  
 $We$  Weber number, eqn (7-3)  
 $X$  coordinate, eqn (8-17)  
 $z$  axial coordinate  
 $\alpha$  thermal diffusivity...

$\alpha'$	absorptivity
$\alpha_0$	thermal diffusivity of water
$\beta$	volumetric coefficient of expansion
$\epsilon$	emissivity, eqn (8-2)
$\theta$	contact angle, eqn (7-1)
$\mu$	coefficient of dynamic viscosity
$\rho$	density
$\rho'$	reflectivity
$\sigma$	surface tension (Section 7)
	Stefan Boltzmann constant (Section 8)
$\tau$	transmissivity, eqn (8-6)
$\phi$	size parameter, eqn (9-1)

### Subscripts

avg	average value
ax	axial direction
C	conduction and convection effect
f	evaluated for the food
i	evaluated at radial node i
j	evaluated at axial node j
l	liquid
m	medium of interest
max	maximum value
min	minimum value

N            evaluated at the outer radial node  
R            radiative effect  
rad          radial direction  
s            solid  
t            total  
v            vapor  
w            evaluated at the wall,  
1,2          evaluated at surface 1 or 2, respectively

Superscript

n            evaluated in the  $n^{\text{th}}$  time increment

## 6.0 INCLUSION OF PHASE CHANGE (MELTING) IN THE THERMAL MODEL

There is usually a substantial energy exchange associated with a phase change. For example, water evaporates relatively slowly from an open, heated, pan because 897.5 Btu of energy (at 14.7 psia) must be supplied to each pound of liquid at 212F to produce a pound of vapor at 212F. Hence, considerable energy exchange takes place with no temperature increase (at constant pressure).

Similarly, when ice is required, liquid water is placed in a region (e.g., the freezing compartment of a refrigerator) where the temperature is well below the freezing point (32F at 14.7 psia). Even after the temperature of the liquid drops to 32F considerable time elapses while the necessary energy is withdrawn (approximately 143 Btu/lbm) from the water to cause a phase change from liquid to solid. Conversely, when the frozen water (ice) is melted, this same energy (143 Btu/lbm), called the latent heat of fusion, must be supplied in addition to the energy which results in the elevation of temperature, called the sensible heat, in a single phase.

### 6.1 The Thermal Model

The thermal model employed thus far (Section 2.3; Ref: Part I) considers only sensible heating of the food and neglects all latent heating (i.e., phase changes). For initial temperatures above 32F (at 5 psia) and cut-off temperatures below 162F (at 5 psia), the model is correct. However, when initially frozen food is heated, considerable error can be introduced by neglecting the amount of energy required to melt the food. This effect was first mentioned in Section 4.4 of Part I. To account for the



latent heat of fusion the original thermal model described in Sections 2 and 3 of Part I was modified.

In the finite difference solutions, the food was subdivided into thirty-six (6-radial and 6-axial subdivisions) toroidal nodes (Fig. 4.2; Ref: Part I). (The centerline nodes are actually cylinders.) The product of the volume of a given node, its density, and its latent heat of fusion is the amount of energy required to transform the node from a 32F solid (ice) to a 32F liquid. In the case of an initially frozen food the temperature of each node is monitored. At the time that the average temperature of a given node reaches 32F a record is begun of the net energy transferred into the node (i.e., the difference between energy entering and leaving). This net energy can be expressed for node (i, j) as:

$$q_{\text{net } i, j} = \Delta q_{i, j} = q_{\text{in } i, j} - q_{\text{out } i, j}$$

$$q_{\text{net } i, j} = 2\pi k \frac{\Delta z}{\Delta r} \left[ r_{i+\frac{1}{2}} (T_{i+1, j} - T_{i, j}) - r_{i-\frac{1}{2}} (T_{i, j} - T_{i-1, j}) \right]$$

$$+ 2\pi r_i k \frac{\Delta r}{\Delta z} \left[ T_{i, j+1} - 2T_{i, j} + T_{i, j-1} \right]. \quad (6-1)$$

The temperature of the node is maintained at 32F until the net energy into the node equals the energy required to melt the nutrient material which the node represents:

$$2\pi r_i \Delta z \Delta r \rho h_{if} = \sum_{n=\tau_1}^{\tau_2} q_{\text{net } i, j} \Delta t^{(n)} \quad (6-2)$$

where  $\tau_1$  is the time increment at which the node first reaches 32F,  $\tau_2$  is the time increment at which sufficient energy has been supplied to melt the node and  $h_{if}$  is the latent heat

(energy) of fusion.

## 6.2 Results

The analysis described in Section 6.1 has been applied to the Skylab thermal, food-heating model. Each of the thirty-six nodes was monitored. Once the temperature of a given node reached 32F it was retained at that level until sufficient heat was supplied to melt it. The temperature then became a dependent variable in the system again.

The thermal properties of the food can change substantially as a result of a phase change. In particular, as seen in Table 6-I, the thermal diffusivity decreased by an order of magnitude from the solid to the liquid state. The higher value would correspond to a faster heating rate. In the model, only one (liquid) value of the thermal diffusivity is used. This fact could lead to a significant discrepancy between the heating times predicted by the model and the actual heating times. However, the discrepancy is not so great as it might appear. First, heating time in the frozen state is a relatively small portion of the total heating time. Also, the food melts first near the heated surface. Thus the thermal diffusivity quickly drops to the liquid value. This liquid partially insulates the rest of the food. Heat is not effectively dissipated from the wall region. It heats up and cuts off the heater in much the same manner as it would even if the proper thermal diffusivity were used for the solid state. Hence, the model is conservative in this respect, but not significantly.

Figure 6.1 illustrates the effect of the inclusion of the phase change. Both average and cold-spot temperatures are plotted against time for both models for the large can. The broken line indicates the heater is cycling. The times required to reach an

TABLE 6-I

## THERMAL PROPERTIES OF SELECTED SKYLAB FOODS [10]

Food Substance	Water Content (%)	Density (lb <sub>m</sub> /ft <sup>3</sup> )	Latent Heat of Fusion (Btu/lb <sub>m</sub> )	Specific Heat (Btu/lb <sub>m</sub> -F)		Thermal Conductivity (Btu/hr-ft-F)		Thermal Diffusivity (ft <sup>2</sup> /hr)	
				**	†	**	†	**	†
Prebuttered Roll	23.8*	15.*	34.	0.70	0.34	0.19	0.45	0.018	0.088
Coffee Cake	25.0*	15.*	36.	0.70	0.34	0.19	0.46	0.018	0.088
Filet Mignon	63.2*	58.	91.	0.71	0.40	0.26	0.97	0.0063	0.042
Chili with Meat	66.9*	58.	96.	0.74	0.40	0.26	0.99	0.0061	0.043
Prime Rib of Beef	72.4*	59.	104.	0.78	0.42	0.27	1.04	0.0059	0.042
Lobster Newburg	75.5*	59.	109.	0.80	0.43	0.28	1.09	0.0059	0.043
Stewed Tomatoes	88.4*	61.	129.	0.91	0.47	0.30	1.25	0.0054	0.044

\* Experimentally determined for actual Skylab foods

\*\* Unfrozen

† Frozen

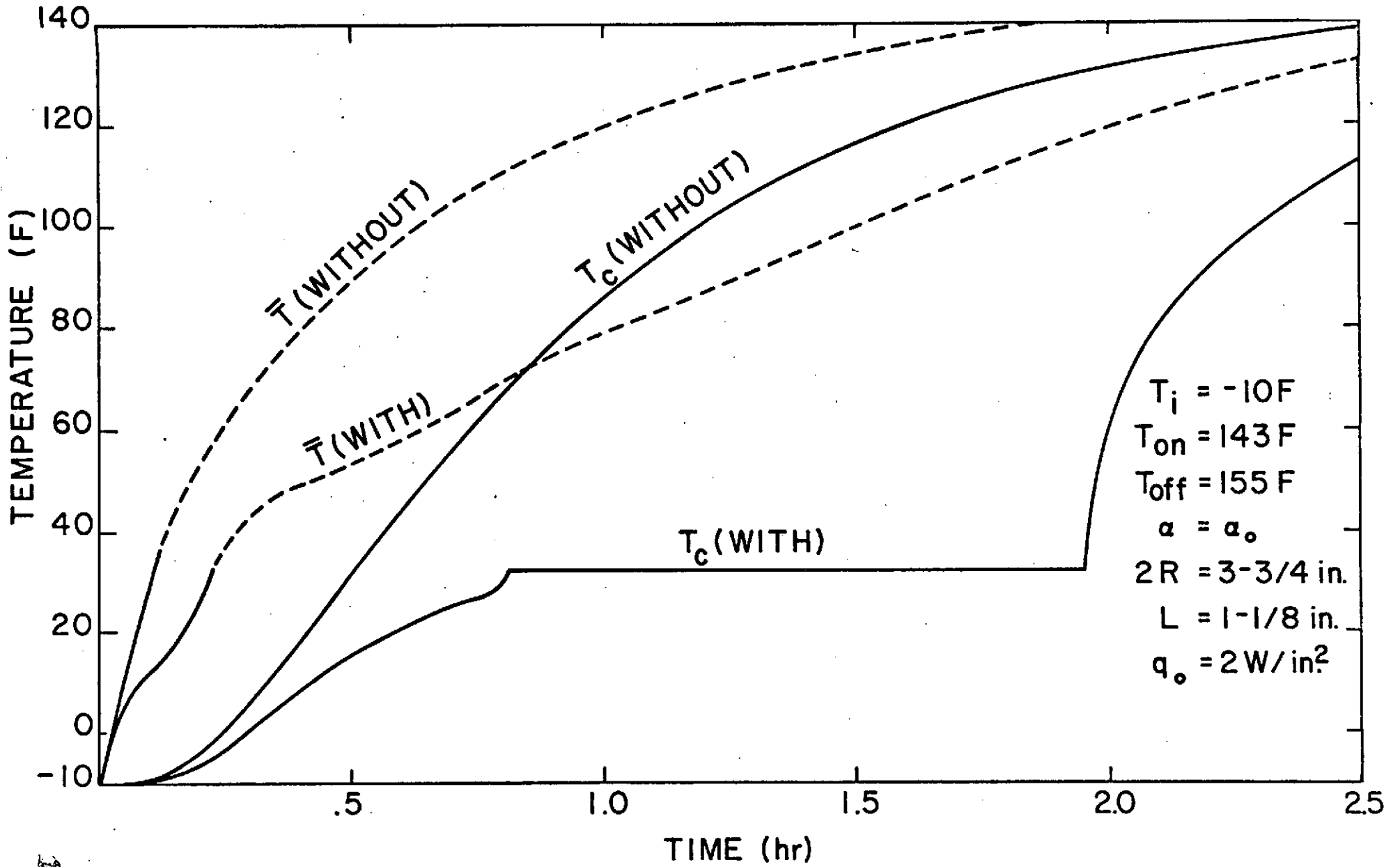


Fig. 6.1: Effect of Phase Change on Temperature Response

average temperature of 130F are approximately 1.35 hours (sensible heating only) and 2.35 hours (phase change included) - an additional 1.0 hours.

In Section 4.4, it was estimated that an additional 0.39 hours would be required if it were assumed that the heater element was uncontrolled (on continuously) for the additional time. Since about  $2\frac{1}{2}$  times as much time is required it can be seen that the heater is actually on only about 40% of the additional time.

## 7.0 LOW-GRAVITY CONSIDERATIONS

In a low-gravity environment fluids do not necessarily settle to the "bottom" of their containers. Instead they may "float" within the container. The loss of direct contact with the walls can significantly effect the heat transfer. Therefore in low-gravity situations fluid behavior is an important consideration in heat transfer analysis.

Strictly speaking, the term zero gravity does not mean that the gravitational force is zero but rather that all net external forces acting on the system are zero. External forces other than gravity acting on a space vehicle are solar forces (pressure), centrifugal forces (due to vehicle rotation), thrust forces and aerodynamic drag forces. Table 7-I provides a summary of typical forces acting on a spacecraft. Space vehicles

TABLE 7-I. Typical Accelerations in a Space Vehicle [11].

<u>SOURCE</u>	<u>CONDITIONS</u>	a/g <sub>0</sub>
1. Solar Pressure	Low absorptance surface	10 <sup>-10</sup>
2. Centrifugal (vehicle rotation)		
(a) to maintain vehicle parallel to earth surface	Low earth orbit	10 <sup>-6</sup>
	High earth orbit	10 <sup>-8</sup>
(b) limit cycle to maintain vehicle oriented towards sun or star	Angular velocity = 0.05 deg/sec;	10 <sup>-8</sup>
3. Thrust for ullage control or from radioisotope propulsion	Thrust = 10 lbf	10 <sup>-4</sup>
4. Aerodynamic drag (C <sub>D</sub> = 2)	Altitude = 100 N mi.	10 <sup>-6</sup>
	250 N mi.	10 <sup>-8</sup>
	400 N mi.	10 <sup>-9</sup>

experience small accelerations at all times even if only that associated with solar pressure alone.

Knowledge concerning the behavior of fluids in low-gravity environments is based in a large part on experimental evidence. Low-gravity environments can be achieved by several test techniques: (a) drop tower, (b) aircraft trajectory, (c) magnetic forces and (d) spacecraft. The majority of low-gravity heat transfer data to date has resulted from drop-tower tests (with aircraft data a distant second).

### 7.1 Liquid/Gas Orientation

In studying the behavior of fluids in low-gravity environments, a knowledge of the predominant forces affecting the fluid must be established. In an Earth environment, the gravitational forces dominate surface-tension forces, and liquids settle to the bottom of containers and gasses collect above. In low-gravity environments, surface tension forces may dominate.

The surface tension of a liquid is dependent not only on the liquid itself but also on the surrounding environment (e.g., the surface tension of water exposed to air is different from the surface tension of water exposed to its own vapor or to some other liquid like alcohol). Liquids are characterized as either "wetting" or "non-wetting" (as illustrated in Fig. 7.1). The contact angle  $\theta$  is expressed in terms of the surface tensions between the liquid and vapor  $\sigma_{lv}$ , the liquid and solid  $\sigma_{ls}$  and the vapor and solid  $\sigma_{vs}$  by the relation [12]

$$\theta = \cos^{-1} \left( \frac{\sigma_{vs} - \sigma_{ls}}{\sigma_{vl}} \right) . \quad (7-1)$$

A completely wetting liquid has  $\theta = 0^\circ$ , and a completely non-wetting liquid has  $\theta = 180^\circ$ . Since surface-tension forces are

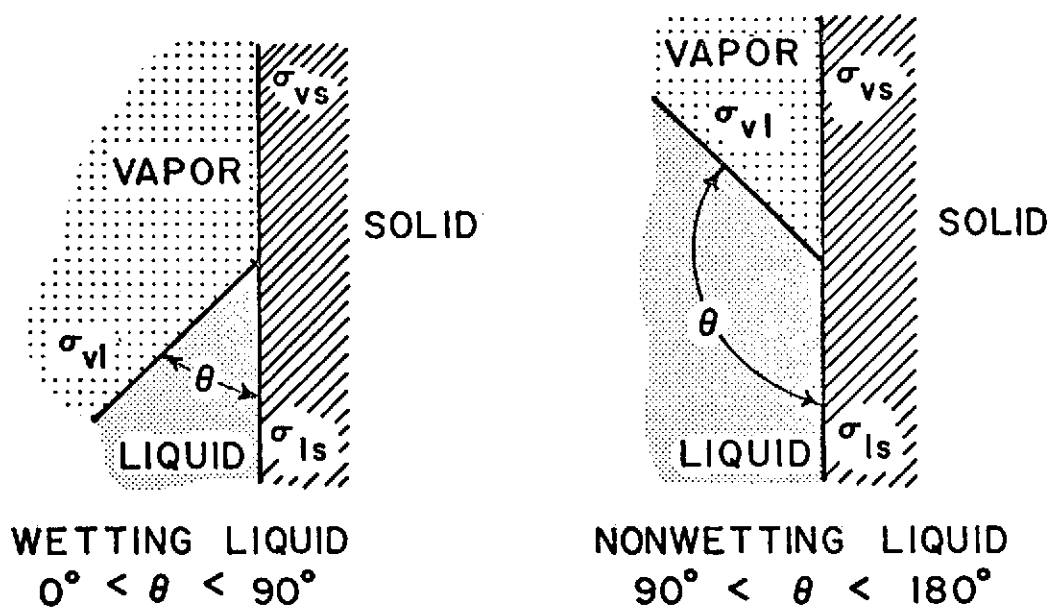


Fig. 7.1: Contact Angle for Wetting and Non-Wetting Liquids

molecular in nature and are independent of gravitational fields, the contact angle  $\theta$  is not changed in low-gravity environments. Drop tests performed by Petrash [13] verify this theory; sketches showing the configuration of "wetting" and "non-wetting" liquids of various contact angles are presented for a cylindrical container in Fig. 7.2, for situations where the container is 50% and 90% filled with liquid in a zero-g environment. Since water is a totally "wetting" liquid, it can be reasonably assumed that nutrient substances would resemble the characteristics of alcohol in Fig. 7.2. It should be pointed out that the gas pocket would not necessarily be at the "top", since the concept of "top" and "bottom" are meaningless in zero-g.

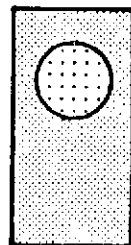
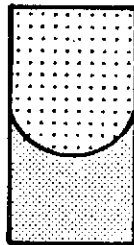
A dimensionless parameter relating the gravitational (or acceleration) forces to the surface tension forces is the Bond number,



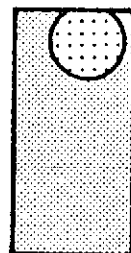
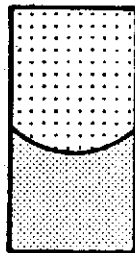
Fig. 7.2: Liquid/Vapor Interface Configuration in Cylindrical Containers During Weightlessness

☐ VAPOR    ☐ LIQUID

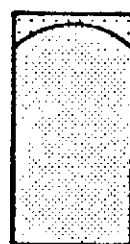
50% FULL    90% FULL



ALCOHOL ( $\theta = 0^\circ$ )



TETRABROMOETHANE ( $\theta = 40^\circ$ )



MERCURY ( $\theta = 125^\circ$ )

$$Bo \equiv \frac{\rho L^2 a}{\sigma} \quad (7-2)$$

As the Bond number increases above unity, the gravitational (or acceleration) forces become more dominant, and the liquid is "settled". As the Bond number decreases below unity, surface-tension forces become more dominant. The surface-tension characteristics then determine the relative position of the liquid and vapor in the container.

Another dimensionless parameter involving surface tension is the Weber number

$$We \equiv \frac{\frac{1}{2} \rho \bar{V}^2 L}{\sigma} \quad (7-3)$$

which is the ratio of the inertia (or dynamic pressure) forces to the surface-tension forces. Again, if the Weber number is greater than unity, the flow or inertia forces become dominant. Figure 7.3 shows graphically the three flow regimes [12]. A Froude

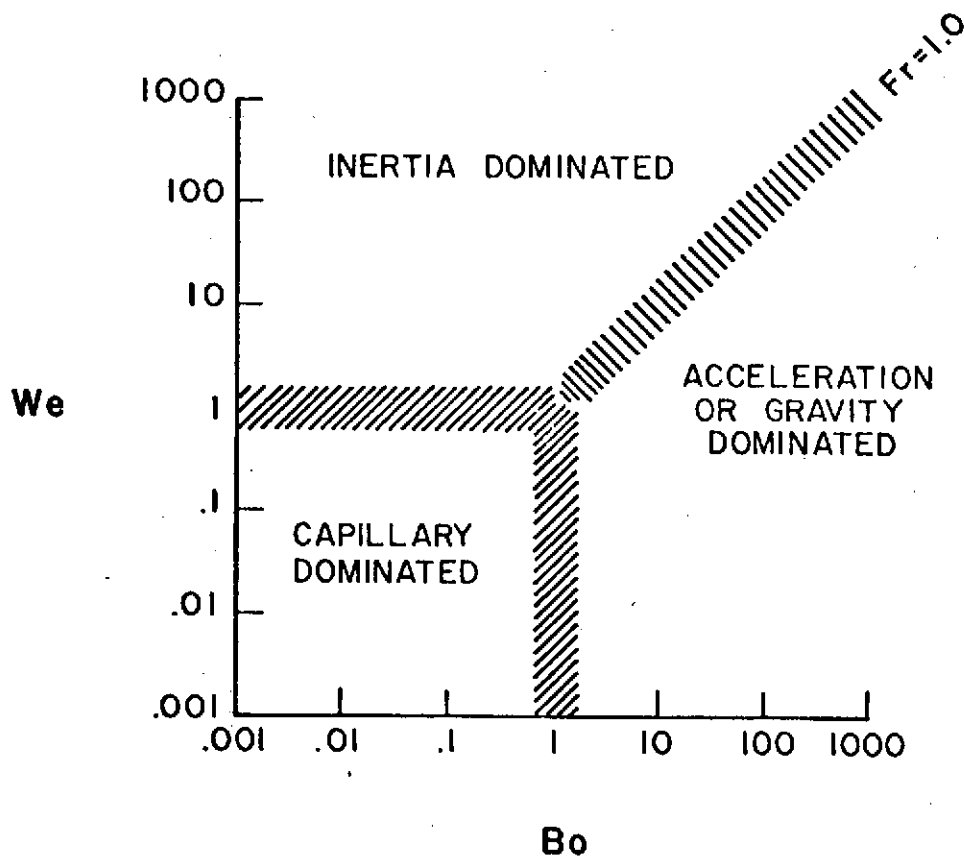


Fig. 7.3: Flow Regimes

number (equal to the square root of the ratio of Weber to Bond number) of unity, i.e.,

$$Fr = \sqrt{\frac{We}{Bo}} = \frac{\bar{V}}{\sqrt{aL}} = 1 \quad (7-4)$$

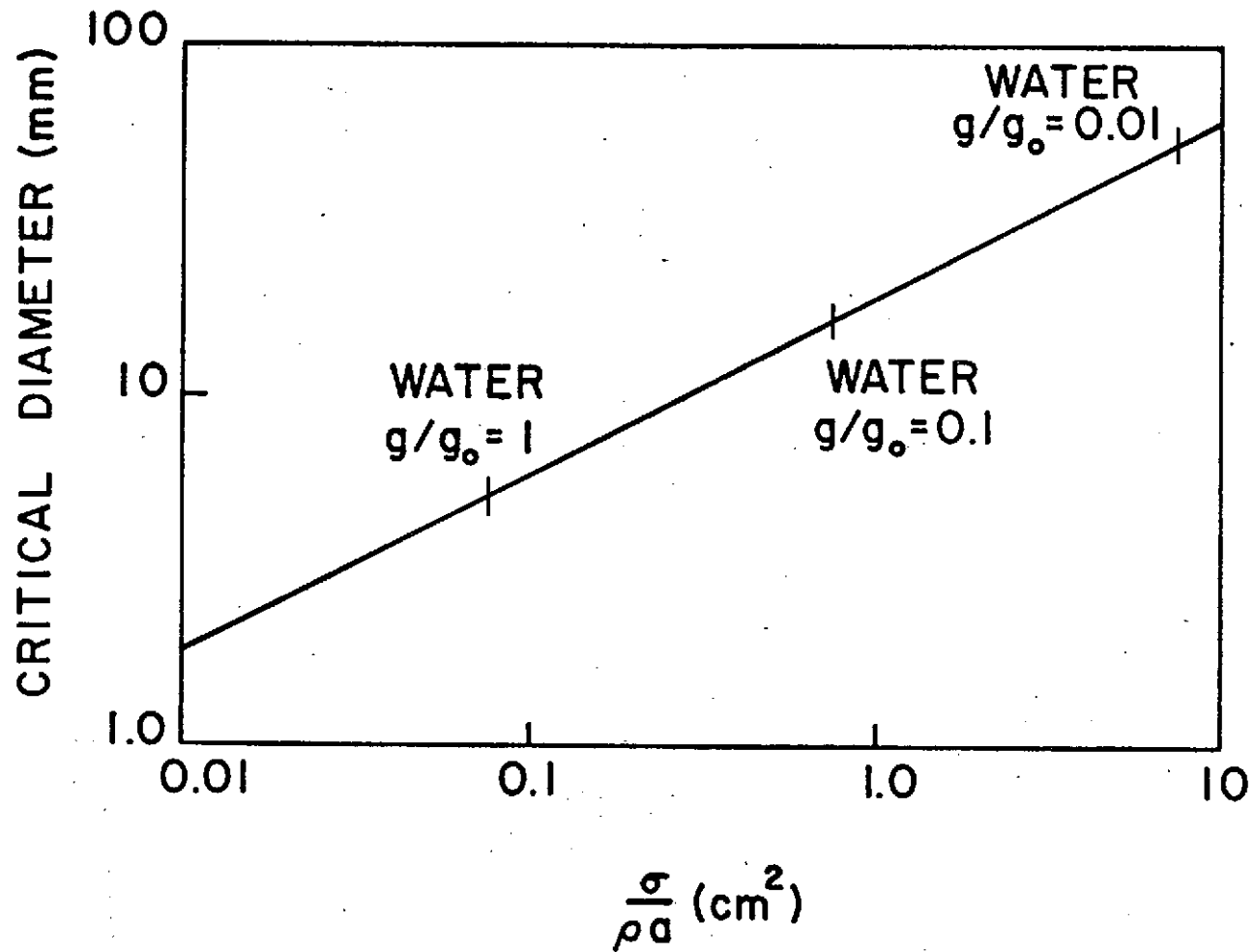
separates the inertia-dominated region from the gravitational (or acceleration)-dominated region. The transition between regimes is gradual and the selection of a Bond number of unity to indicate transition is only approximate.

Instability in the liquid/vapor interface has been observed at various specific values of the Bond number - the critical Bond number. Critical Bond numbers appear in the literature ranging from 0 to 15 depending on the geometry and the substances involved. The critical Bond number (determined from one-g tests) can be extrapolated to lower gravity levels (based on the results of Otto [12] for cylindrically shaped containers). For a given interface (e.g., air and water) and a given critical Bond number, eqn (7-2) defines a value for the critical characteristic dimension,  $L$ , for the system. (This dimension must have been specified in the evaluation of the critical Bond number.) For a cylindrical container this dimension is the diameter. The critical diameter for a water/water-vapor interface in a cylinder ( $\sigma/\rho = 73 \text{ cm}^3/\text{sec}^2$ ) at various gravitational levels is shown in Fig. 7.4.

## 7.2 Low-Gravity Heat Transfer

In a zero-gravity environment, there are no free-convection currents as a result of bouyancy. The dominant mode of heat transfer should be the conduction mechanism, although some fluid motion may occur as a result of temperature gradients. The significant dimensionless parameter in low-gravity heat transfer is the Rayleigh number  $Ra$  which is the product of the Grashof number  $Gr$  and Prandtl number  $Pr$

Fig. 7.4: Predicted Critical Diameter of Water Based on Bond Number



$$Ra = GrPr = \frac{g\beta c \rho^2 L^3 (T_w - T_b)}{k\mu} \quad (7-5)$$

The Grashof number is the ratio of buoyant forces to viscous forces. The Prandtl number is the ratio of momentum diffusivity to thermal diffusivity. High Grashof numbers indicate significant buoyant (free convection) forces, and high Prandtl numbers indicate significant molecular activity (hence convection) with respect to thermal conduction. Hence the value of the Rayleigh number can be used to indicate the relative importance of convection to conduction.

For a gas in a spherical container at low pressure, Tyler [14] found no significant contribution from the convection mechanism for Rayleigh numbers less than 650. For a fluid layer confined between two horizontal plates and heated from below, the convection is suppressed when the Rayleigh number (based on the thickness of the layer  $w$ ) is below 1700 [15]; this critical value was verified experimentally for water as the fluid. As a numerical example [15] with  $w = 0.1$  ft (1.2 in.) and a temperature difference of 100F, convection currents are induced in water if  $g/g_0 > 3.2 (10^{-5})$ . This example does not differ substantially from the specific cases of interest. If the upper surface layer were not bounded by a solid surface but by a free surface, the Rayleigh number must be below approximately 1100 for the conduction mechanism to dominate. Eckert investigated vertical layers of fluid, which may represent a tall cylinder enclosed by two plates of height  $L$  separated by a distance  $w$ ; the top and bottom were insulated. The regime of pure conduction ended at  $Ra = 500 L/w$  where the Rayleigh number uses the characteristic length  $w$  [15].

For a surface dissipating a uniform heat flux per unit area

$q''$ , a modified Rayleigh number  $Ra^*$  involving the Nusselt number  $Nu$  is employed

$$Ra^* = GrPrNu = \frac{g\beta c \rho^2 L^4 q''}{k^3 \mu} \quad (7-6)$$

For heated vertical surfaces, the modified Rayleigh number characterizes the various flow regimes according to [11]:

$Ra^* < 1$  Conduction dominated

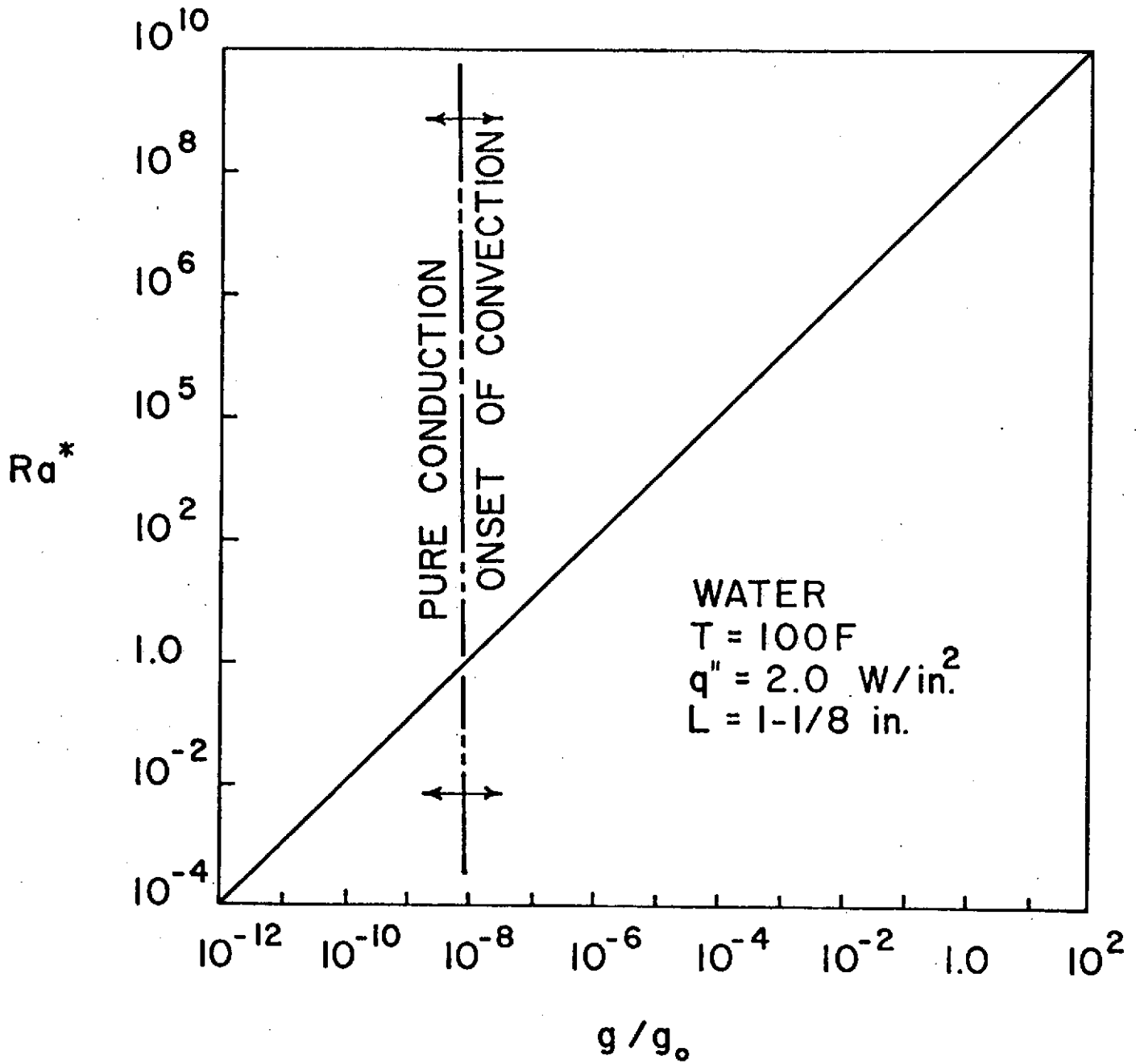
$10^3 < Ra^* < 10^5$  Viscous Flow

The modified Rayleigh number is shown in Fig. 7.5 as a function of the fraction of Earth's gravity  $g/g_0$  for water at 100F for the special case where  $q'' = 2.0 \text{ W/in}^2$  and  $L = 1-1/8 \text{ in}$ . Since the onset of convection currents is directly related to the Rayleigh number, as the magnitude of the gravitational forces are reduced, the convection regime is delayed.

### 7.3 Laboratory Simulation of Reduced Gravity

Siegel [15] discusses the laboratory simulation of increased or decreased gravity fields by rescaling the size of the experiment. Since the Rayleigh number is the important parameter including the gravitational forces, the effects of changes in the gravitational field can be simulated by altering the characteristic length  $L$ . For the isothermal heating surfaces, the Rayleigh number depends on the product  $gL^3$ ; for the uniform surface heat flux, the modified Rayleigh number depends on the product  $gL^4$ . Therefore, in simulating an increased or decreased gravity environment by rescaling the size of Earth based experiment, the dimensions of the experimental test apparatus must be multiplied by the factor  $(g/g_0)^{1/3}$  or  $(g/g_0)^{1/4}$ , respectively. In simulating reduced gravity, the laboratory experiment would be scaled down.

Fig. 7.5: Onset of Convection Currents Based on Modified Rayleigh Number



## 8.0 ALTERNATE MODEL

No real surface is perfectly smooth. Even a polished surface has microscopic irregularities. When two surfaces are brought together then, the actual contact area is only a fraction of the apparent contact area due to the surface roughness as depicted in Fig. 8.1.

Conduction heat transfer depends on a conducting medium and is proportional to the cross-sectional area (Fourier's law). Due to the reduced effective area, conduction heat transfer between two surfaces in contact is reduced from the level expected if no interface were present. This phenomenon is usually analyzed in terms of an effective "thermal contact resistance." The reduced cross-sectional area can be viewed as an increase in the resistance to the transfer of heat by conduction.

If the narrow space between the surfaces is evacuated, radiation is the only mode of heat transfer available to transport heat between parts of the surfaces not in contact. If the space contains a gas, then all modes of heat transfer (conduction, convection, and radiation) are present. However, the thermal conductivities of gases are negligible compared to the thermal conductivities of most solids. Only a relatively small amount of heat is conducted through the gas. The smallness of the gap between the surfaces usually restricts convection currents severely. (In true zero-g, of course, no currents exist.) Hence, convection heat transfer is usually insignificant. Therefore, even with a gas present, radiation is usually the dominant mode of heat transfer across the gap. (Depending on the percent of the actual contact, the conduction directly between the surfaces may still be the single, most significant transport mechanism.)



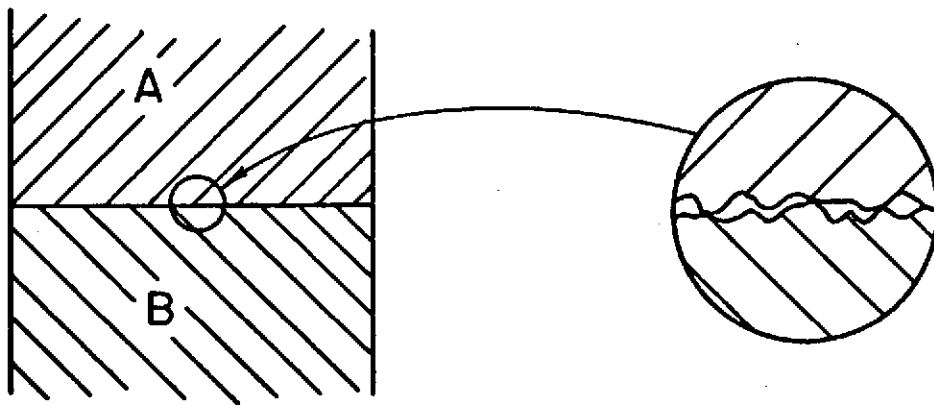


Fig. 8.1: Contact Area

### 8.1 Contact Resistance in Skylab Heater

There are two possible areas where significant contact resistance could be encountered in the Skylab configuration: First, the contact between the food can and the cavity wall; and second, between the food itself and the can wall. Of the two, the latter is potentially more critical. The separation of the food from the wall due to zero-g effects has been discussed in Section 7. Also, the plastic bag containing the food within the can could substantially reduce contact area if wrinkling should occur.

While the simple reduction of heat transfer to the food due to poor contact is certainly significant, a potentially far more important problem, related to contact resistance, is present; in the actual tray, the heater-control thermocouple is located in the wall of the cavity. Due to poor thermal contact between the food and the wall in the vicinity of the sensor, the cavity wall may heat significantly faster than the rest of the wall which maintains contact with the food. (There is no place for the heat to go.) In this case, the sensor responds to a temperature which is not representative of the system as a whole. The sensor temperature is much higher; the heater is turned off prematurely. Since heat is not dissipated from the area of the sensor effectively, the heater remains off for an extended time. The food heating process can, therefore, be delayed simply because the heater is not activated as intended.

### 8.2 Equivalent Thermal Properties

Inclusion of all the aspects in the problem of contact resistance discussed in Section 8.1 would require a rather complex model. In addition, the values of some of the governing

parameters are simply not known. For example, the actual contact area may be a function of time. An extensive analysis is therefore not justified. The following is a discussion of the analysis required to generate a reasonable model.

The contact resistance between the can and cavity wall is neglected. If the food does draw away from the can, the separation is over the "ring area" ( $2\pi r_N(\Delta z)$ ) associated with the basic discretization scheme discussed in Section 4. (This assumes axial symmetry.) The energy is then transported from the outer radial node (this is the toroidal node depicted in Fig. 8.2) to the adjacent food node by radiation and conduction through the nitrogen gas used to fill the can. Since there is no food at the wall, the outer radial node corresponds to the wall plus the space between the wall and the food. Axial heat transport to and from this node is therefore equivalent to axial conduction in the wall.

The radial radiation/conduction transport and the wall axial conduction can be put into a form which can be used in conjunction with the original model. This is accomplished by determining equivalent thermal conductivities and heat capacities which account for the phenomenon discussed and by using them directly in a non-isotropic "conduction" model.

**8.2.1 Equivalent Conductance due to Radiation:** The radiation exchange between the can wall and the food is approximated by the exchange between two parallel walls of emissivities (equal to absorptivities),  $\epsilon_1$  and  $\epsilon_2$ . This model is approximate; however, due to the other uncertainties and simplifications in the model, a more complex radiation model is not justified.

The net radiation exchange between any two surfaces is usually expressed in the form:

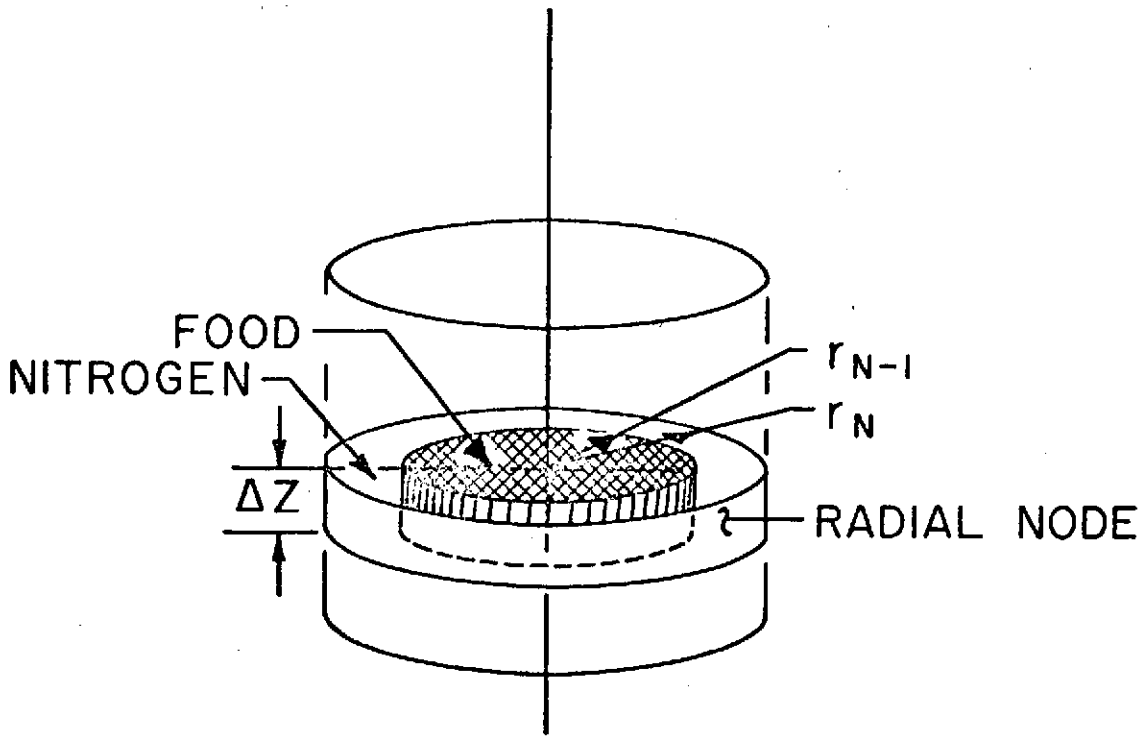


Fig. 8.2: Outer Radial Node

$$q_{R_{1-2}} = J_1 A_1 F_{1-2} - J_2 A_2 F_{2-1} \quad (8-1)$$

where  $J$  is the radiosity (total radiation which leaves a surface per unit time and per unit area) and  $F_{1-2}$  and  $F_{2-1}$  are the radiation configuration factors (e.g.,  $F_{1-2}$  is the fraction of energy leaving surface 1 which reaches surface 2).

The radiosity is therefore the sum of the energy emitted and the energy reflected (with no transmitted energy), or

$$J = \epsilon E_b + \rho' G \quad (8-2)$$

where  $\epsilon$  is the emissivity,  $E_b$  the blackbody emissive power ( $\sigma T^4$  in radiative equilibrium),  $\rho$  the reflectivity, and the  $G$  the irradiation (total radiation incident upon a surface per unit time and per unit area).

The configuration factor is a geometry-dependent variable. For exchange between large parallel walls  $A_1 = A_2$ ,  $F_{1-2} = F_{2-1} = 1$  (since all the radiation leaving either surface strikes the other surface), and

$$G_1 = J_2 ; G_2 = J_1 \quad (8-3)$$

Therefore, in thermal equilibrium

$$J_1 = \epsilon_1 \sigma T_1^4 + (1-\epsilon_1) J_2 \quad (8-4)$$

$$J_2 = \epsilon_2 \sigma T_2^4 + (1-\epsilon_2) J_1 \quad (8-5)$$

where

$$\rho' = 1 - \alpha' - \tau = 1 - \alpha' = 1 - \epsilon \quad (8-6)$$

(transmissivity,  $\tau$ , is zero, and  $\alpha' = \epsilon$  in thermal equilibrium by Kirchhoff's law). From eqns (8-4) and (8-5)

$$J_1 = \frac{\epsilon_1 \sigma T_1^4 + (1-\epsilon_1) \epsilon_2 \sigma T_2^4}{1 - (1-\epsilon_1)(1-\epsilon_2)} \quad (8-7)$$

$$J_2 = \frac{\epsilon_2 \sigma T_2^4 + (1-\epsilon_2) \epsilon_1 \sigma T_1^4}{1 - (1-\epsilon_1)(1-\epsilon_2)} \quad (8-8)$$

Substitution of eqns (8-7) and (8-8) into eqn (8-1) together with the assumptions of exchange between parallel walls

$$\frac{q_{R1-2}}{A} \Big|_{\substack{\text{parallel} \\ \text{walls}}} = \frac{\sigma(T_2^4 - T_1^4)}{\frac{1}{\epsilon_1} + \frac{1}{\epsilon_2} - 1} \quad (8-9)$$

Furthermore,

$$T_2^4 - T_1^4 = (T_2 - T_1)(T_2 + T_1)(T_2^2 + T_1^2) \quad (8-10)$$

so that if  $T_1 \cong T_2 = \hat{T}$

$$T_2^4 - T_1^4 \cong 4\hat{T}^3 (T_2 - T_1) \quad (8-11)$$

This approximation is commonly called the "linearizing approximation" for radiation exchange. For

$$0.9 < T/\hat{T} < 1.1 \quad (8-12)$$

the error in eqn (8-11) is less than 12%. For the initially frozen food (largest temperature range)  $\hat{T}$  is chosen as

$$\hat{T} = \frac{150 + |-10|}{2} = 80 \text{ F} = 540 \text{ R} \quad (8-13)$$

so that

$$\frac{450}{540} = .84 < \frac{T}{\hat{T}} < 1.13 = \frac{610}{540} \quad (8-14)$$

From eqn (8-9) then

$$\frac{q_{R1-2}}{A} \Big|_{\substack{\text{parallel} \\ \text{walls}}} \cong \frac{4\hat{T}^3 \sigma}{\frac{1}{\epsilon_1} + \frac{1}{\epsilon_2} - 1} (T_2 - T_1) \quad (8-15)$$

or

$$\frac{q_{R1-2}}{A} \Big|_{\substack{\text{parallel} \\ \text{walls}}} = k_e \frac{(T_2 - T_1)}{(X_2 - X_1)} \quad (8-16)$$

where

$$k_{e_R} = \frac{4\sigma T^3 (X_2 - X_1)}{\frac{1}{\epsilon_1} + \frac{1}{\epsilon_2} - 1} \quad (8-17)$$

is an equivalent conductivity and  $X$  represents the coordinate measured perpendicular to the surface. Equation (8-16) casts the radiative heat transfer between parallel walls into the form of a "conduction model" (Fourier's law).

**8.2.2 Radial Equivalent Conductance:** If true conduction and/or convection heat transfer through the medium between the walls is significant, these mechanisms can also be put into this same form (eqn (8-16)). The effects of conduction and convection are usually combined into a single effective conductivity (a technique for enclosed spaces, e.g. [16])

$$\frac{q_{C_{1-2}}}{A} \Big|_{\text{parallel walls}} = k_{e_C} \frac{(T_2 - T_1)}{(X_2 - X_1)} \quad (8-18)$$

where  $k_{e_C}$  is an equivalent conductivity due to conduction and convection and can be found [16] correlated as a function of Grashof number for free convection situations.

In space, with no free convection, only conduction through the intervening medium is present and

$$k_{e_C} = k_m \quad (8-19)$$

where  $k_m$  is simply the thermal conductivity of the medium.

The conduction and radiation represent parallel paths for heat transfer. The total heat transfer then is

$$\frac{q_{C_{1-2}}}{A} + \frac{q_{R_{1-2}}}{A} = k_{e_C} \frac{(T_2 - T_1)}{(X_2 - X_1)} + k_{e_R} \frac{(T_2 - T_1)}{(X_2 - X_1)}$$

$$= \left( k_{e_C} + k_{e_R} \right) \frac{(T_2 - T_1)}{(X_2 - X_1)} \quad (8-20)$$

$$\frac{q_{T_1-2}}{A} = k_e \frac{(T_2 - T_1)}{(X_2 - X_1)} \quad (8-21)$$

where

$$k_e = k_{e_C} + k_{e_R} \quad (8-22)$$

is the equivalent total conductance of the medium. From eqns (8-17), (8-19) and (8-22)

$$k_e = \frac{4\sigma T^3 (X_2 - X_1)}{\frac{1}{\epsilon_1} + \frac{1}{\epsilon_2} - 1} + k_m \quad (8-23)$$

**8.2.3 Wall Equivalent Conductance:** The sixteen outer nodes (4-side, 5-top, 5-bottom, and 2-corner described in Section 4.4) represent either food plus wall or nitrogen gas plus wall depending upon whether the food has separated from the wall (Fig. 8.3). The radial heat transfer from the "side" nodes and axial heat transfer into the food from the top and bottom nodes is handled with the concept of equivalent conductivity discussed in Section 8.2.1. The heat transferred along the wall is now considered.

Heat is transferred axially between the wall nodes (N,j) and (N,j+1) (Fig. 8.4) by two parallel paths — along the container wall and through the food (or gas if the food has separated). The wall-plus-nitrogen or wall-plus-food routes therefore form parallel paths for heat conduction. The heat conducted along the two paths between the two side nodes (N,j) and (N,j+1) is

$$q_w = A_w k_w \frac{T_{N,j+1} - T_{N,j}}{z_{j+1} - z_j} \quad (8-24)$$



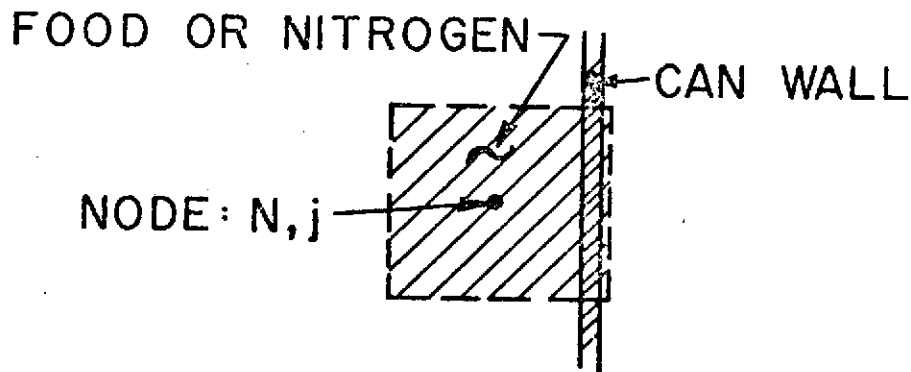
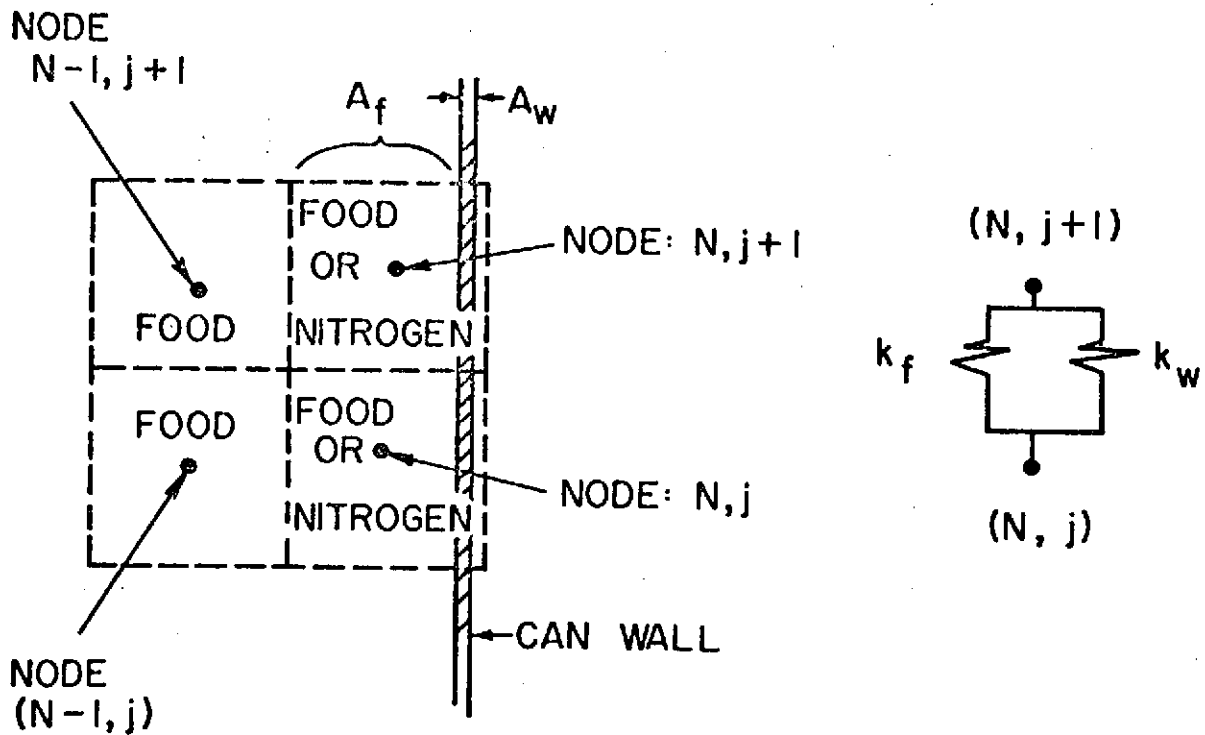


Fig. 8.3: Outer Radial Node



a) Actual Path

b) Equivalent Path

Fig. 8.4: Model for Axial Conduction

$$q_f = A_f k_f \frac{T_{N,j+1} - T_{N,j}}{z_{j+1} - z_j} \quad (8-25)$$

where  $A_w$  and  $A_f$  are the cross-sectional areas for axial heat transfer in the wall and food (or nitrogen), respectively, and  $k_w$  and  $k_f$  are the thermal conductivities of the wall and food (or nitrogen), respectively. From the electrical analogy for heat conduction (or from an independent derivation) the equivalent conductance for the parallel paths is

$$k_{e_{ax}} = \frac{A_w k_w + A_f k_f}{A} \quad (8-26)$$

where  $A = A_w + A_f$ . The total heat transfer between nodes  $(N,j)$  and  $(N,j+1)$  is then

$$\frac{q}{A} \mid (N,j) \text{ to } (N,j+1) = \frac{A_w k_w + A_f k_f}{A} \frac{T_{N,j+1} - T_{N,j}}{z_{j+1} - z_j} \quad (8-27)$$

$$A = 2\pi \left( r_N - \frac{r_N + r_{N-1}}{2} \right) (z_{j+1} - z_j)$$

Similarly for two adjacent nodes on the bottom of the can

$$\frac{q}{A} \mid i,0 \text{ to } i+1,0 = \frac{A_w k_w + A_f k_f}{A} \frac{T_{i+1,0} - T_{i,0}}{r_{i+1} - r_i} \quad (8-28)$$

**8.2.4 Equivalent Heat Capacity:** In the model developed in earlier sections, each node had the same heat capacity. (Actually, the thermal diffusivity,  $\alpha = k/\rho c$  was specified. The changes in the value of the thermal conductivity,  $k$ , have already been discussed in Section 8.3. The density,  $\rho$ , and the specific heat,  $c$ , always appear in this analysis as a product. This product is called heat capacity.) Since the previous model was homogeneous (modeling the food only) this assumption was

valid. However, the current model includes regions of food, voids, and can wall. The heat capacity must now be specified at each node individually. In particular, the equivalent heat capacities of the sixteen boundary nodes must be determined. This is easily accomplished by using the volume weighted average of the heat capacities of the constituents of the node

$$(\rho c)_e = \frac{\sum_{m=1}^N \rho_m c_m V_m}{\sum_{m=1}^N V_m} \quad (8-29)$$

where the subscript  $m$  indicates the different materials composing the node.

### 8.3 A Constant Wall-Temperature Model

The model used so far has included a simulation of the on/off temperature control heater. This type of boundary condition significantly increased the complexity of the model over that used in an earlier study [17]. It was felt, however, that its inclusion was necessary. Now, with the concept of equivalent thermal properties already developed in this section, it will be shown that the added complexity of this heat flux boundary condition is unnecessary and that a constant-temperature boundary condition adequately describes the physical system. This simplification results only when the aluminum can wall is included within the outer food node.

In the following discussion, attention is directed to a typical outer node (i.e., one that includes the wall). Rather than include the details of the analysis of all possible wall nodes (e.g., top, center, corner, side, bottom, etc.), only a side-wall node is discussed. Therefore, axial heat transfer is parallel to the wall, and radial heat transfer is perpendicular to the wall. It is with this limitation (side wall node) that

the subscripts "rad" (radial) and "ax" (axial) are used in this section. The concepts developed here are general and can, of course, be extended to other nodes. Only the details would differ.

8.3.1 The Case for the Constant Wall-Temperature Model: The aluminum can is formed of rolled aluminum sheet (nominal thickness 0.01 in.). The cross-sectional area available for axial conduction along the wall for the larger can is (see Fig. 8.4)

$$A_w = 2\pi R t_w = 2\pi \frac{3^{3/4}}{2} 0.01 = 0.118 \text{ in.}^2$$

where  $t_w$  is the wall thickness. For axial conduction in the outer food node, the cross-sectional area is

$$A_f \cong 2\pi \left(R - \frac{\Delta r}{2}\right) \Delta r = 3.4 \text{ in.}^2$$

The thermal conductivities for the aluminum wall  $k_w$  and for the food  $k_f$  are

$$k_w \cong 130 \text{ Btu/(ft-hr-F)}$$

$$k_f \cong k_{\text{water}} \cong 0.3 \text{ Btu/(ft-hr-F)}$$

Then from eqn (8-26)

$$k_{e_{ax}} = \frac{\frac{.118}{144} (130) + \frac{3.4}{144} (0.3)}{3.5/144} \cong 4.7 \text{ Btu/(hr-ft-F)} \quad (8-30)$$

If the food separates from the wall,  $k_f$  becomes the thermal conductivity of the replacement gas. The equivalent conductance for axial heat transfer is essentially unaffected since as seen in eqn (8-30), a decrease in the value of  $k_f$  (e.g., to 0.02 Btu/(ft-hr-F) for nitrogen) causes no significant change in the value of  $k_{e_{ax}}$ .

However, the equivalent conductance for radial heat transfer is significantly affected if the food separates from the wall. With no separation, the equivalent conductance for radial heat transfer is simply the thermal conductivity of the food, i.e.,

$$k_{e_{\text{rad}}} = k_f \cong k_{\text{water}} \cong 0.3 \text{ Btu}/(\text{ft-hr-F}) \quad (8-31)$$

If the food does separate from the wall, the equivalent conductance is due to the combined effects of conduction and radiation across the gap. If the effect of the plastic inner liner is neglected, eqn (8-23) can be used. For

$$\hat{T} \cong 600 \text{ R}$$

$$\epsilon_1 = \epsilon_w \cong 0.2$$

$$\epsilon_2 = \epsilon_f \cong 1.0$$

$$x_2 - x_1 = \frac{\Delta r}{2} = 3/16 \text{ in.}$$

$$k_m = k_{\text{nitrogen}} \cong 0.02 \text{ Btu}/(\text{ft-hr-F})$$

$$k_{e_{\text{rad}}} = \frac{4(.1714) \times 10^{-8} (600)^3 \frac{3/16}{12}}{1/0.2 + 1/1.0 - 1} + 0.02$$

$$\cong 0.01 + 0.02 = 0.03 \text{ Btu}/(\text{ft-hr-F}) \quad (8-32)$$

It is evident by the relative sizes of the contributions to  $k_{e_{\text{rad}}}$  that radiative heat transfer in the gap is about one half as effective as conduction in the gas.

From Fourier's law the equivalent axial and radial heat transfer are, respectively,

$$q_{\text{rad}} = k_{e_{\text{rad}}} A_{\text{rad}} (\Delta T)_{\text{rad}} = k_{e_{\text{rad}}} 2\pi R (\Delta z) (\Delta T)_{\text{rad}} \quad (8-33)$$

$$q_{\text{ax}} = k_{e_{\text{ax}}} A_{\text{ax}} (\Delta T)_{\text{ax}} = k_{e_{\text{ax}}} 2\pi R (\Delta r) (\Delta T)_{\text{ax}} \quad (8-34)$$

When eqns (8-30), (8-31), (8-32), (8-33) and (8-34) are combined

$$q_{\text{rad}}_{\text{no sep}} \cong 0.005 (\Delta T)_{\text{rad}} \quad (8-35)$$

$$q_{\text{rad}}_{\text{sep}} \cong 0.0005 (\Delta T)_{\text{rad}} \quad (8-36)$$

$$q_{\text{ax}} \cong 0.1 (\Delta T)_{\text{ax}} \quad (8-37)$$

Due to the overwhelming preference for conduction along the wall over conduction from the wall (by comparison of eqn (8-37) with both eqn (8-35) and eqn (8-36)), it should be expected that the wall temperature should remain fairly uniform, even over the unheated portion (top). Also, because conduction from the wall is so severely inhibited, the wall should heat up quickly.

The time required to heat the can wall to the cut-off temperature can be estimated if it is assumed that all the heat added initially is used in heating the wall only.

The volume of the aluminum wall (large can)

$$V_w = 2\pi R L t_w + 2\pi R^2 t_w \cong 0.35 \text{ in}^3$$

For an initial temperature of -10 F the heat required to raise the wall temperature to 155 F is

$$Q_w = \rho_w V_w c_w (\Delta T)_w \cong 1.15 \text{ Btu}$$

The side and bottom of the food is exposed to the heater so that the heated area is

$$A_w = 2\pi R L + \pi R^2 \cong 25 \text{ in}^2$$

The heater supplies 2 W/in<sup>2</sup>. While the heater is activated, the heating rate is

$$q_{\text{max}} = 2 \text{ W/in}^2 (25 \text{ in}^2) \cong 170 \text{ Btu/hr} \quad (8-38)$$

The time required to heat the walls from - 10 F to 150 F is

$$t = \frac{Q_w}{q_{\max}} \approx 25 \text{ sec.} \quad (8-39)$$

This represents the minimum time required since some of the heat would go to the food.

In summary then, it would be expected that within the first minute or so of heating the walls should reach the cut-off temperature and remain between  $T_{\text{off}}$  and  $T_{\text{on}}$  for the remainder of the heating process. Therefore, a model using a constant wall temperature between  $T_{\text{off}}$  and  $T_{\text{on}}$  should approximate the physical system reasonably well.

**8.3.2 Initial Results:** Based on the constant wall-temperature model verified in the previous section, a computer simulation was developed. Since all the heat transfer has been modeled as equivalent conduction, the simulation is essentially that for a conduction model with nonisotropic thermal properties. A finite difference algorithm based on the thirty-six node discretization scheme (introduced in Section 4.4, Part 1) was used.

The food was assumed to have the thermal properties of water ( $\alpha/\alpha_0 = 1$ ) and the wall temperature was taken as the average of the two control temperatures ( $T_w = 149 \text{ F}$ ). Figures 8.5 through 8.10 depict the time responses of the cold spot and the average temperatures for initial temperatures of 60 F and - 10 F. The first three figures are for the large can; the last three, for the small can.

The major uncertainty in the analysis to this point is the degree to which (if at all) the food separates from the wall. Because of this uncertainty, simulations were run for three different contact areas (between the food and the wall): (a) no separation (100% contact) (Fig. 8.5 and 8.8); (b) partial

>6E

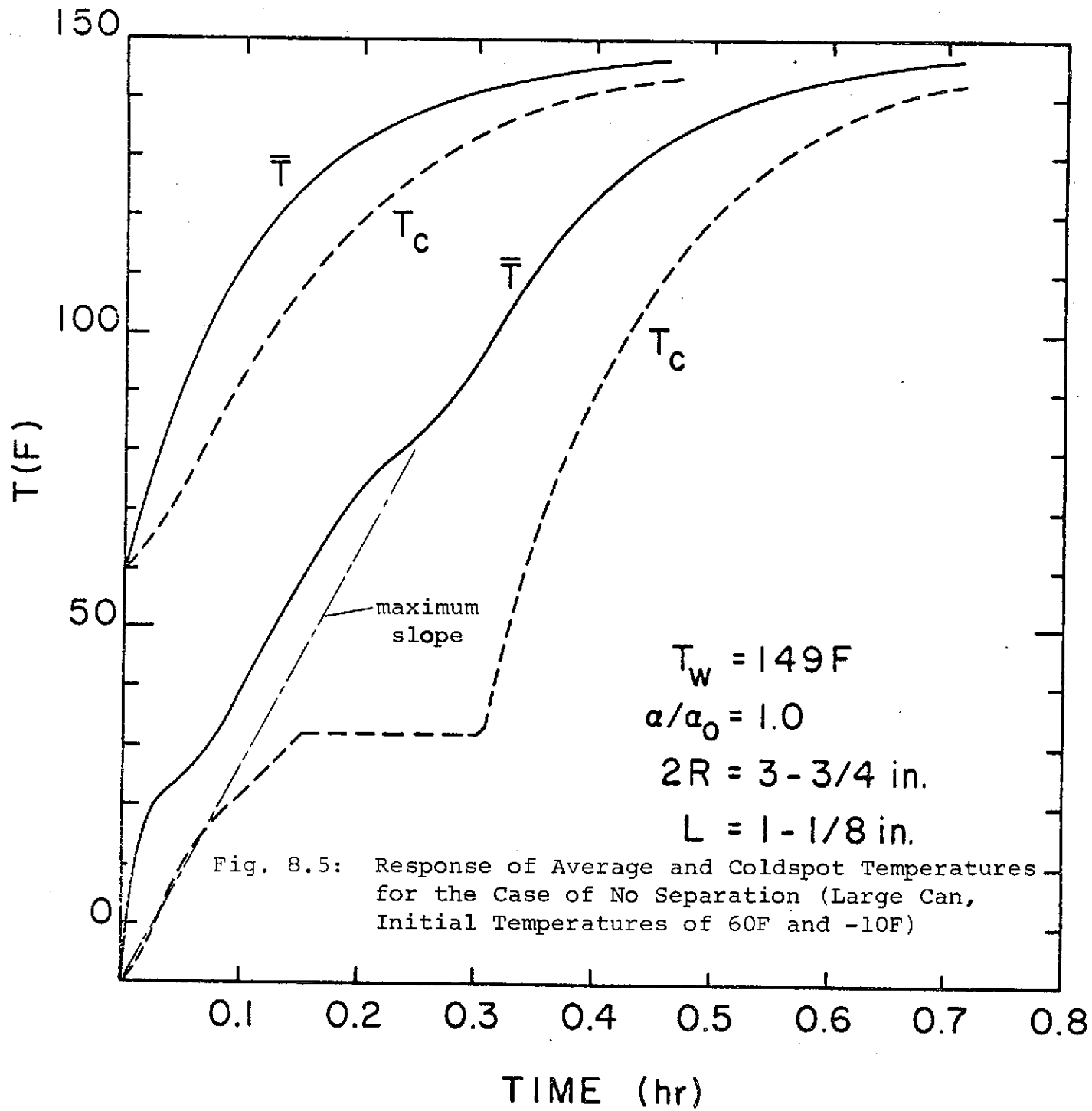
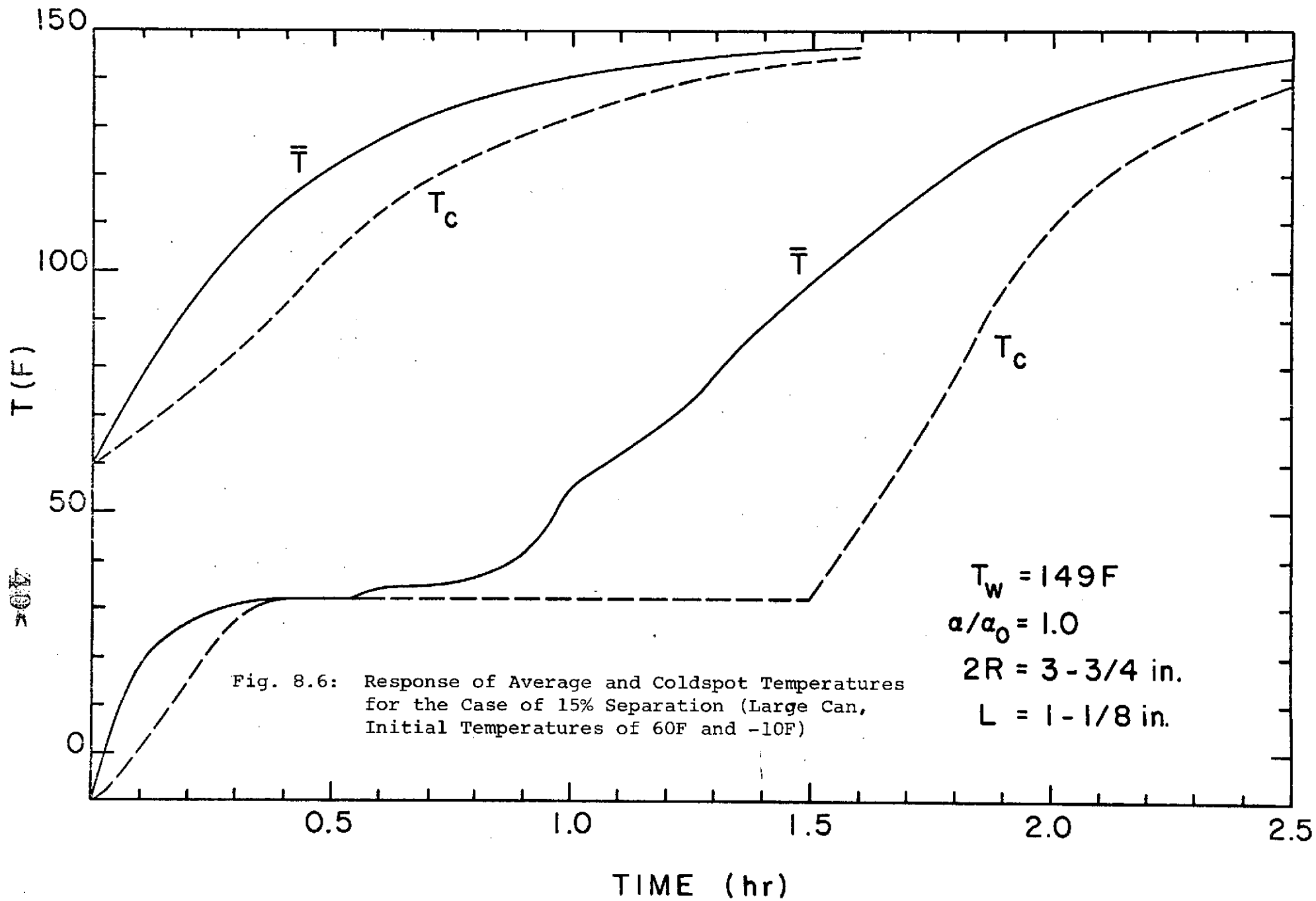
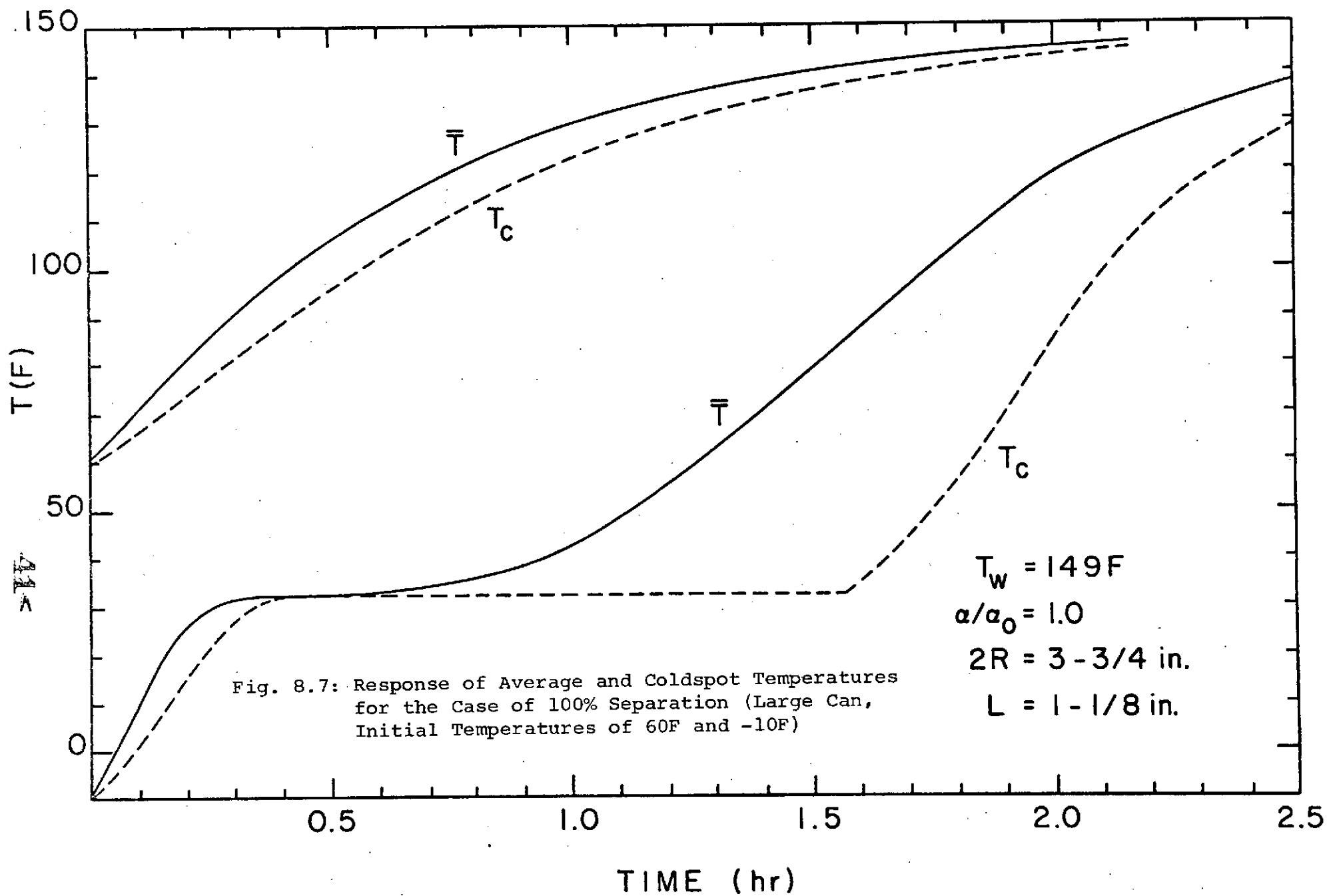


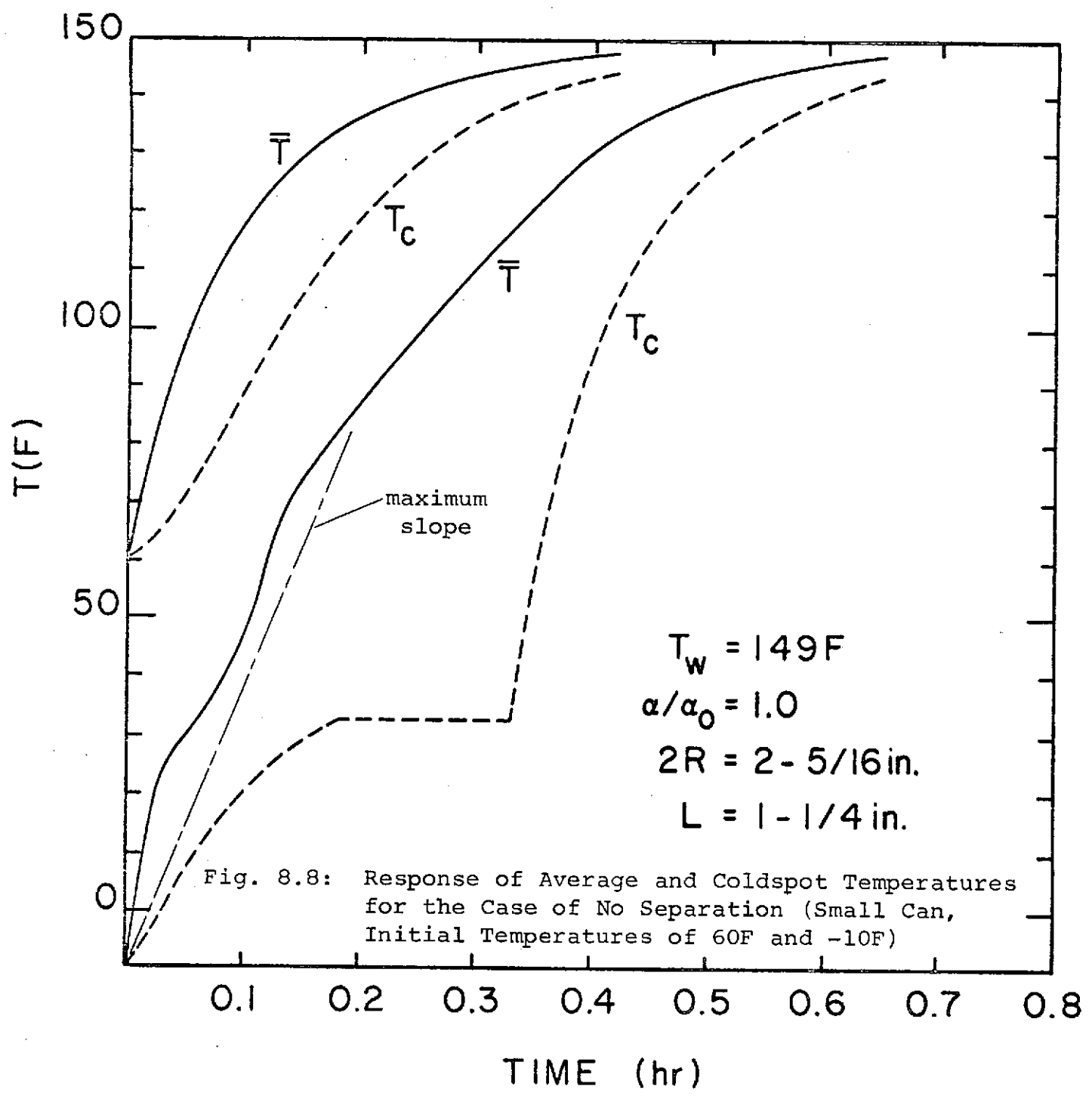
Fig. 8.5: Response of Average and Coldspot Temperatures for the Case of No Separation (Large Can, Initial Temperatures of 60F and -10F)

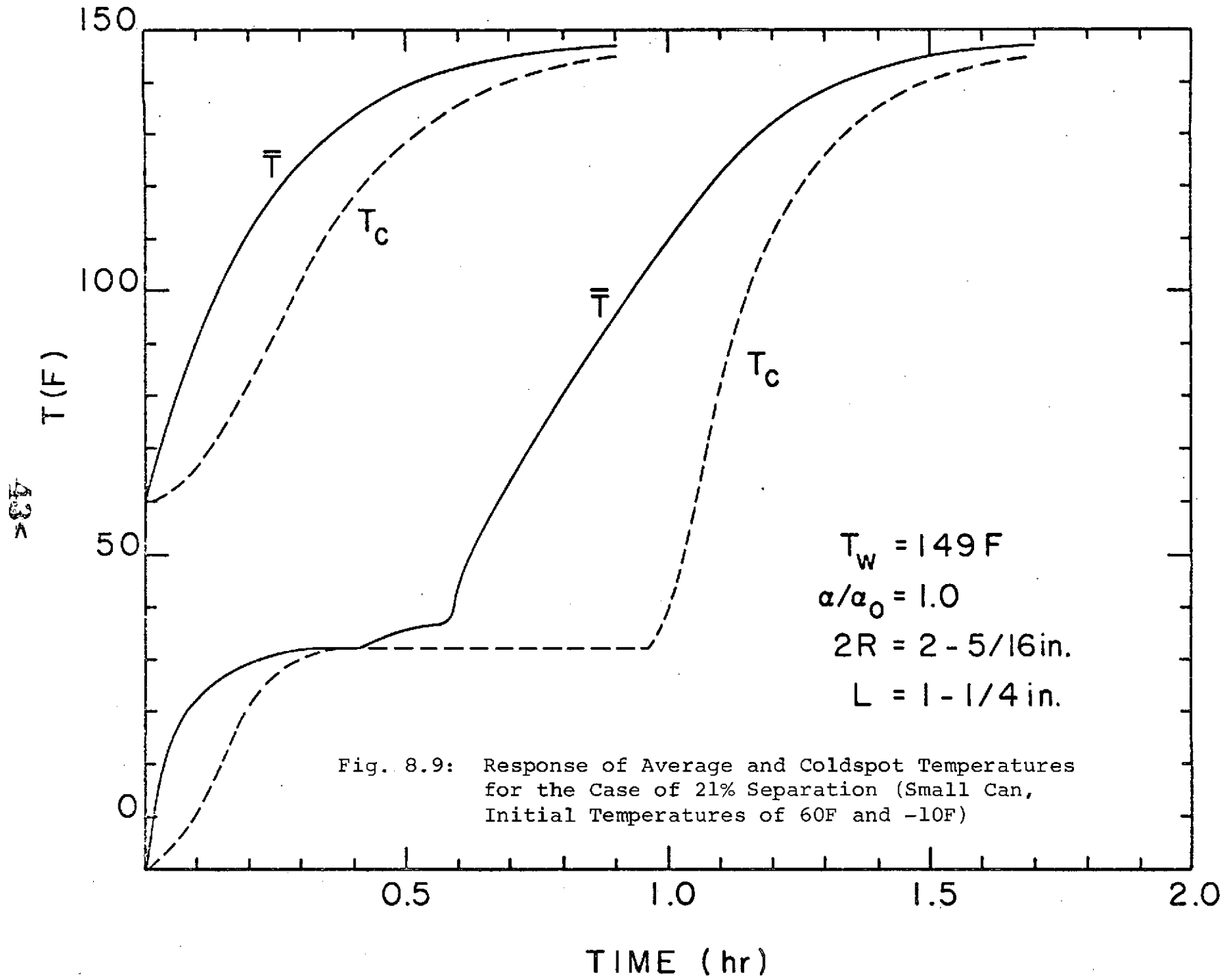


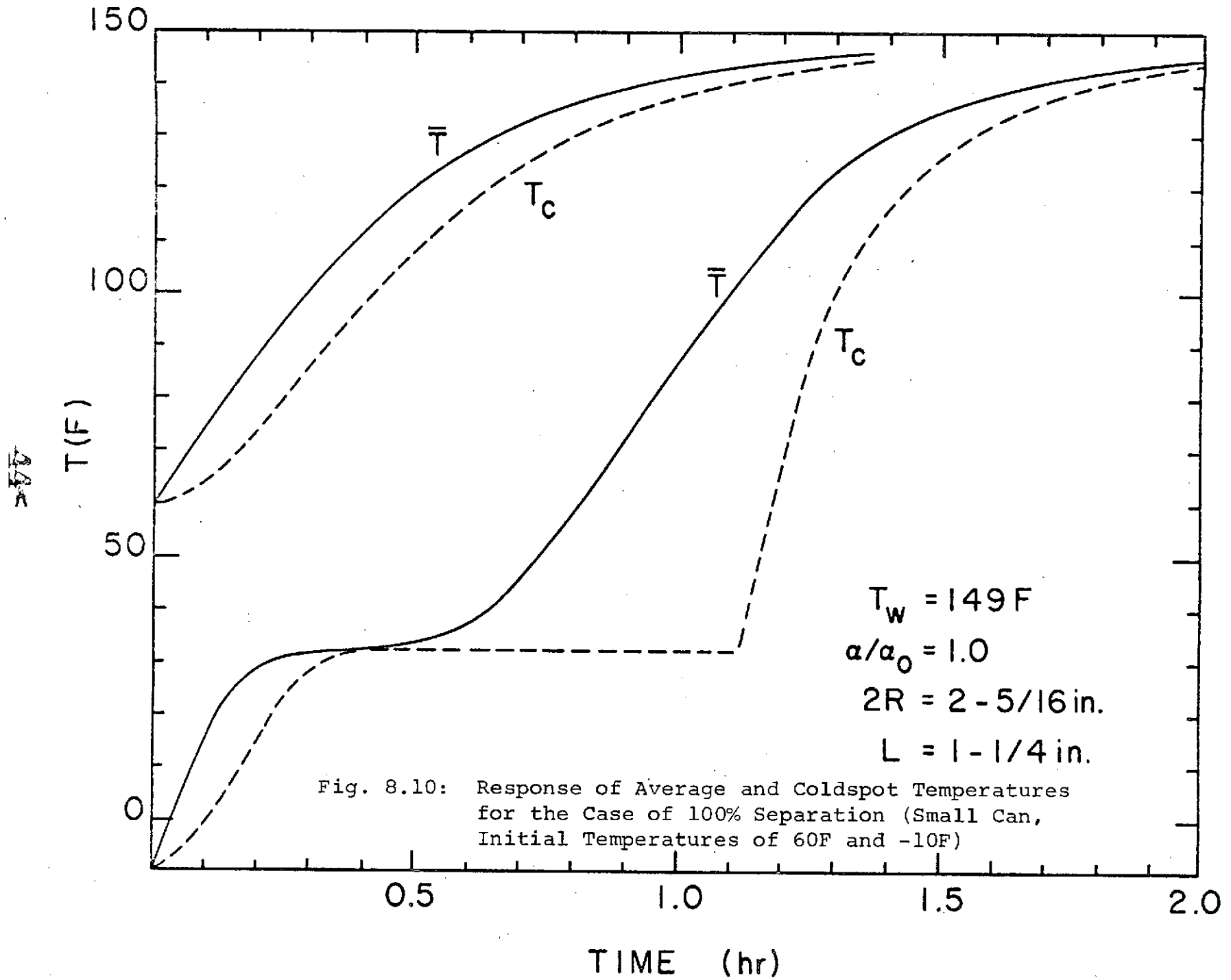




42







separation (from outer wall) (Figs. 8.6 and 8.9); and (c) complete separation (Figs. 8.7 and 8.10).

8.3.3 Corrected Results: The results represented in Figs. 8.5 through 8.10 must now be corrected for two reasons. First, due to the constant-temperature boundary condition, the heat flux at the wall is not controlled in the model. The results obtained must therefore be checked to assure that the wall flux required in the model is less than (or in the limit equal to) that which can be supplied by the heater. Second, in cases where the food separates (totally or partially) from the wall, some of the nodes which previously represented food, now represent nitrogen gas (since there are still thirty-six total nodes). The amount of food heated in the model is therefore less than that actually in the can. The simulation then predicts that the food heats more quickly than in the actual system simply because the model includes less food than the actual system.

8.3.3.1 Correction for Maximum Wall Heat Flux: From eqn (8-38) the maximum rate of heat addition to the large can is 170 Btu/hr (if the heater is activated continuously). Therefore, the food cannot "heat-up" at a rate which exceeds this value.

For the initially unfrozen food ( $T_i = 60$  F), all the heat added is "sensible" (no phase change involved). The maximum rate at which the average temperature could increase can be found by equating the heat absorbed by the food with the maximum dissipation from the heater. In a "small" increment of time,  $\Delta t$ , the average temperature increases by  $\Delta T$ . These two quantities are related through an energy balance

$$\rho V c (\Delta T) = q (\Delta t) \quad (8-40)$$

where  $q$  is the mean heating rate over the time increment,  $\Delta t$ . Therefore, the maximum rate at which the average temperature could increase can be approximated by

$$\left(\frac{dT}{dt}\right)_{\max} \cong \left(\frac{\Delta T}{\Delta t}\right)_{\max} = \frac{q_{\max}}{\rho V c} \quad (8-41)$$

where  $q_{\max}$  is achieved by continuous heating.  $q_{\max}$  was evaluated as 170 Btu/hr for the large can in eqn (8-38). It is 91 Btu/hr for the small can. If the properties of water are used for the food, the maximum instantaneous rates of increase in the average temperature with no phase change are,

$$\left(\frac{dT}{dt}\right)_{\max} \cong 370^{\circ} \text{R/hr} \quad (8-42)$$

large can

$$\left(\frac{dT}{dt}\right)_{\max} \cong 470^{\circ} \text{R/hr} \quad (8-43)$$

small can

The maximum heating rates are expected in the "no separation" cases. The maximum slopes determined in eqns (8-42) and (8-43) are included in Figs. 8.5 and 8.8. A comparison of the maximum slopes to the time response of the average temperature for the initially unfrozen food indicates that in the initial heating period ( $t < 0.05$  hr), the model is being heated at a rate which exceeds the output of the heater. Therefore, the heating time will be extended. However, since this excess heating is indicated for only a short time, the overall heating time should not increase by a significant amount.

For the initially frozen food, the maximum rate at which the average temperature can increase is reduced because a large part of the heat added is required to melt the food. This portion is called the "latent" heat. Equation (8-40) is therefore modified to the form

$$\rho V c (\Delta \bar{T}) + \rho V h_{if} = q(\Delta t) \quad (8-44)$$

As seen in Fig. 8.5 for the large can, the cold spot finally melts after about 0.3 hrs of heating. At this time the average temperature has increased to about 95 F. The average heating rate required over this initial 0.3 hr period is therefore from eqn (8-44)

$$q_{avg} = \frac{\rho V c (105) + \rho V (143)}{0.3} = 400 \text{ Btu/hr}$$

But the maximum heating rate has been established (eqn (8-38)) as 170 Btu/hr. At this lower rate, the minimum time required

$$t_{min} = \frac{.3(400)}{170} \cong 0.7 \text{ hrs}$$

to melt the food completely and raise the average temperature to 95 F is 0.4 hrs more than predicted by the model without a heater flux restraint. It is apparent then that the heating curve should be displaced to at least 1.7 hrs at  $T = 95 \text{ F}$ . Above 95 F, the slope is below the maximum slope without phase change, so it is not expected that further displacement of the time coordinate (beyond 0.4 hrs) would be necessary. A similar analysis for the small can indicates that heating time is delayed at least 0.25 hrs beyond that predicted in the model

As pointed out, these time delays represent the minimum extension possible for the heating process. It is assumed that the heaters remain activated continuously in the initial heating phase. This is realistic and the results are expected to be valid. However, some further delay is possible if the heater is deactivated for any appreciable time in this initial period.

8.3.3.2 Correction for Reduced Volume in Model: As indicated earlier, separation of the food from the walls in the model was



achieved by replacing the appropriate "food" nodes with "nitrogen and wall" nodes. The results depicted in Figs. 8.6, 8.7, 8.9 and 8.10 therefore indicate the temperature response for a food sample which is smaller than the actual one. These results can be used, however, to estimate the temperature for a food sample of the proper size. This is accomplished by assuming that the heating time is increased proportionately with the increase of food mass or volume. Therefore, at a given average temperature, the heating time predicted by the model is multiplied by the ratio of actual food volume to model food volume to determine the corrected time to achieve the given average temperature.

A typical evaluation of this area ratio parameter is presented in Fig. 8.11 which depicts the geometry for the complete separation of food in the large can. The actual food volume is

$$\pi R^2 L = 12.5 \text{ in}^3$$

The model volume is

$$\pi \left( R - \frac{\Delta r}{2} \right)^2 (L - \Delta z) = 8.05 \text{ in}^3$$

The actual volume is therefore

$$\frac{12.5}{8.05} = 1.55 \text{ or } 155\%$$

of the model volume.

The time for the average temperature to reach 110 F (Fig. 8.7) is predicted to be 1.61 hr. The volume correction would indicate that the time should be increased by 55% or to 2.56 hr.

Similar calculations yield volume ratios for the other cases described in the figures. The volume ratios are presented in Table 8-I.

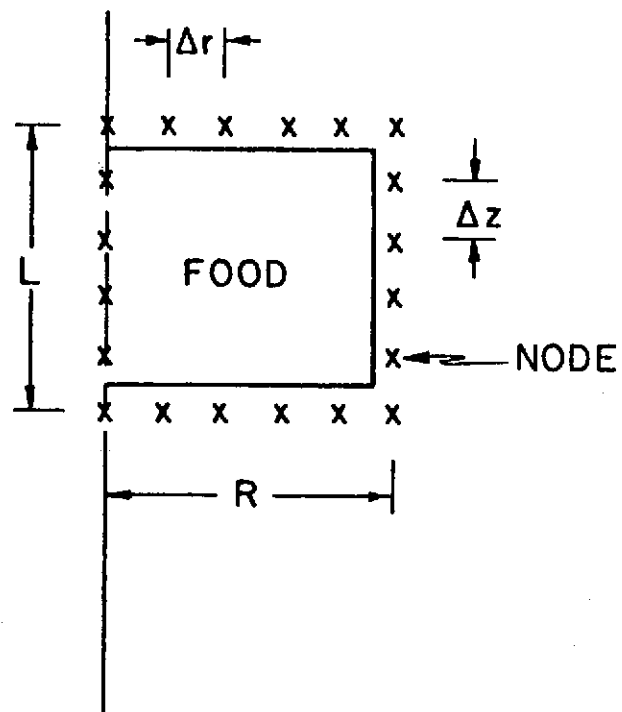


Fig. 8.11: Complete Food Separation

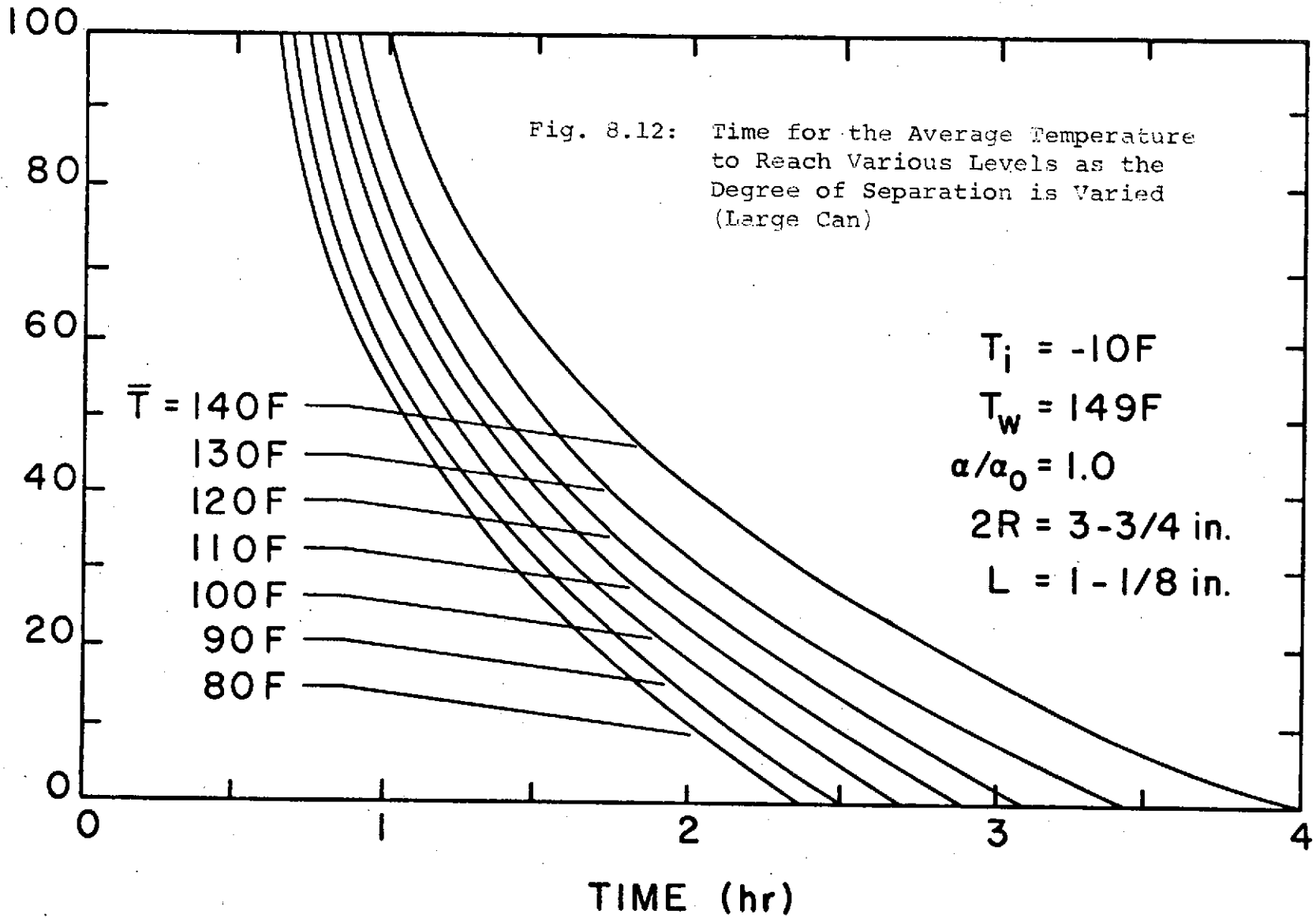
Table 8-I  
Ratio of Actual to Model Volume

<u>Configuration</u>	<u>Volume Ratio</u>
Large Can - complete separation (Fig. 8.7)	1.55
partial separation (Fig. 8.6)	1.15
Small Can - complete separation (Fig. 8.10)	1.61
partial separation (Fig. 8.9)	1.23

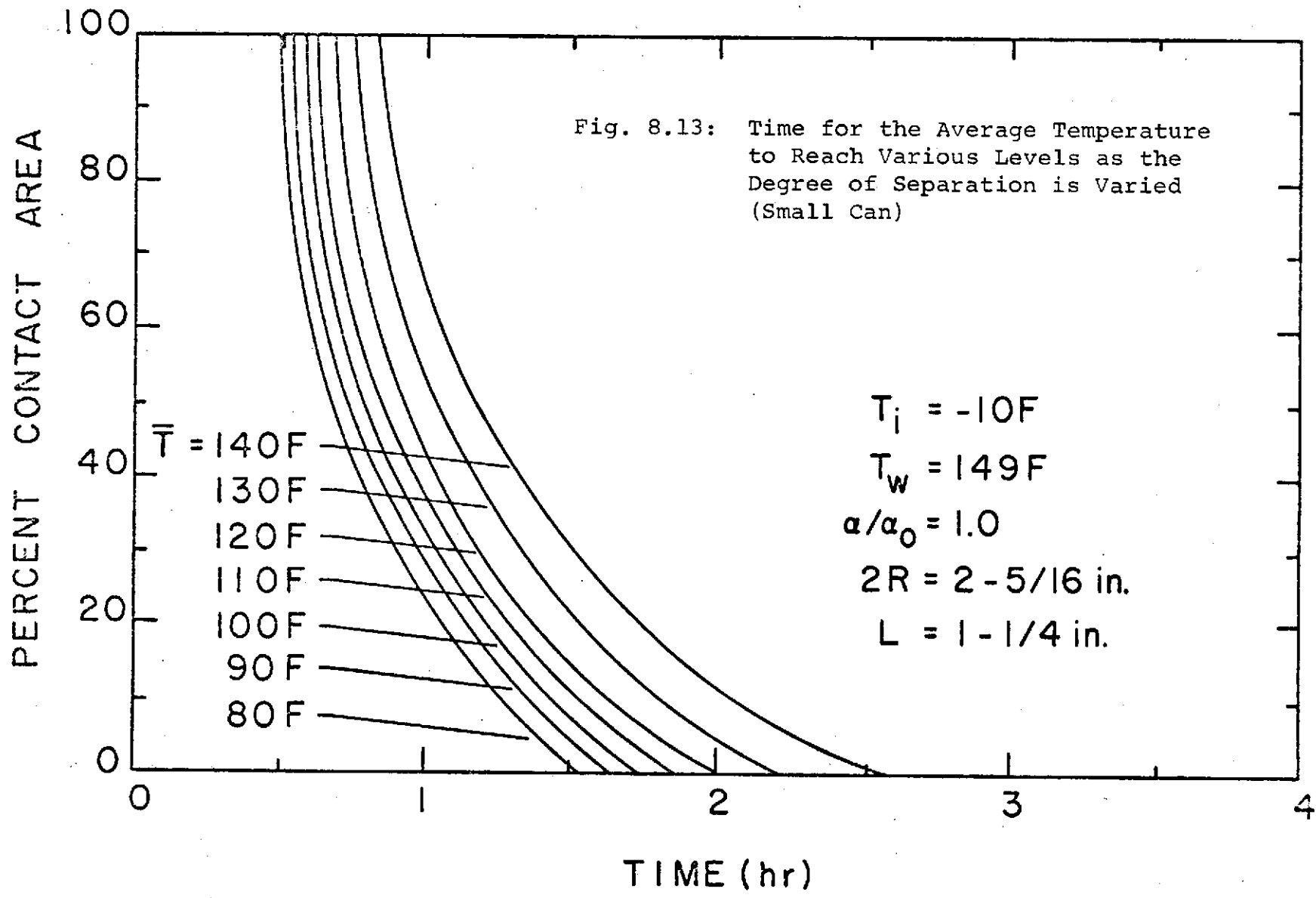
8.3.3.3 Results: While the two corrections discussed in the previous sections are only approximate, they are necessary if full use is to be made of the model. These two corrections (maximum heat flux and volume ratio) were applied to the initial results of Figs. 8.5 through 8.10. The corrected results are contained in Figs. 8.12 and 8.13 for the large and small cans, respectively. In these figures the time for the initially frozen food to reach a given average temperature is plotted against the percent of food-can contact area. (No separation corresponds to 100% contact area, and complete isolation of the food from the wall corresponds to 0% contact area). The wall temperature is fixed at 149 F and the food is given the thermo-physical properties of water. The interesting (and reasonable) result demonstrated in the figures is that a reduction in contact area up to about 50% results in only a moderate increase in heating time. Heating times are, however, significantly extended as complete separation is approached. This general trend should be anticipated if one considers the parallel paths (radiation and conduction through the gas and direct conduction between the food and the wall) available for heat transfer. The direct

512

PERCENT CONTACT AREA



505



conduction is far more effective (comparing eqns (8-35) and (8-36)). As separation begins, most of the heat is still transferred effectively by this path. The decrease in effective cross-sectional area available for direct wall to food conduction is partially off-set by an increase in the temperature difference (food does not heat as fast). However, the incremental gain in temperature difference begins to decrease as separation continues. As complete separation is approached, the severe reduction in the cross-sectional area significantly reduces direct conduction heat transfer; the heat is transferred (less effectively) along the radiation/conduction path. The overall effectiveness of the transfer begins to diminish rapidly until (with total separation) the less effective path is "carrying" the whole heat load.

Due to the fact that the cans are "filled" with food, it is very unlikely that complete or even near-complete separation would occur. If it is assumed that "considerable" separation is unlikely, the constant-temperature boundary condition predicts a somewhat shorter heating time than the intermittent flux boundary condition of the first model. The intermittent flux boundary condition model is therefore judged to be the more conservative model, and it is used in the next section to perform some optimization studies.

## 9.0 OPTIMIZATION

The primary objective of this work was to predict the thermal characteristics of a particular configuration. However, the model provides the tool to pursue parametric studies. These studies are performed by maintaining all but one of the problem parameters at their "standard" values while allowing the remaining one to vary over a range of values. The standard configuration used (except as noted) in the following results is: the large container ( $R = 1-7/8$  in.,  $L = 1-1/8$  in.),  $T_{\text{off}} = 155\text{F}$ ,  $T_{\text{on}} = 143\text{F}$ ,  $q_0 = 2$  W/in<sup>2</sup>,  $\alpha = 0.005633$  ft<sup>2</sup>/hr and an initial temperature of 60F.

An important question to be answered by this study was to determine if the nutrient material lingered in the critical temperature zone (45-140F) for more than two hours. The results are therefore presented in one of two forms: 1) the time response of the average temperature,  $\bar{T}$ , for specific values of a single parameter (e.g., heater power level) and 2) the time required to achieve a given average temperature for a continuous range of values for a given parameter. This second form of presentation allows one to determine quickly the total time for which the average temperature is within the critical range. For example, for a given set of parameters the time required to heat to 90F and to 140F can be determined directly from the graph. The difference in these values is the time interval during which the average food temperature was within that range.

### 9.1 Effect of Thermophysical Properties

The only thermophysical property influencing the temperature response is the thermal diffusivity,  $\alpha$ . (Actually, thermal conductivity does appear in the heat flux boundary condition, e.g.,

eqn (4-15) (Ref: Part I). Since it appears only with  $q_0$ , the effect of its variation can be considered to be a variation in  $q_0$ . The standard value of thermal conductivity is that of water at standard conditions, 0.327 Btu/ft-hr-°F.) The thermal diffusivity for most nutrient materials is close to that of water. However, as previously discussed the reliability of published thermophysical data is questionable. Therefore, instead of using nutrients as parameters (e.g., response time of beef), the dimensionless ratio  $\alpha/\alpha_0$  (where  $\alpha_0$  is the thermal diffusivity of water at standard conditions = 0.005633 ft<sup>2</sup>/hr) is used. Figure 5.1a and 5.1b (Ref: Part I) depict the effect of thermal diffusivity on heating time.

As discussed in Section 6, the thermal model developed does not have the capability of changing the value of thermal diffusivity during a run. Therefore, because the thermal diffusivity is much higher in the frozen state than in the liquid state and since the liquid value is used, the model heats more slowly than the actual food.

## 9.2 Effect of Heater Power Level

If food is heated by a uniform heat source which is not controlled, the heater would remain activated continuously until the desired average temperature of the food had been attained. However, if the food near the heating surfaces is to be kept from boiling, a control mechanism must be included in the heater circuit. The temperature/time relationships for the temperature-controlled heater are compared to the uncontrolled heater in Fig. 5.2a and 5.2b (Ref: Part I). Both the average and "coldspot" temperatures are depicted as a function of logarithmic time. For the large container, the time required to increase the average temperature to



140F is increased from about eleven minutes to over an hour when the heater is controlled.

Figure 9.1 indicates the heating time required to achieve a given average temperature as the heater power level is changed. As seen in the figure, heating times can be significantly increased by increasing the heater flux in the controlled heater only up to about 0.5 W/in<sup>2</sup>. Above that level, increasing the flux level simply inactivates the heater for longer periods of times (Fig. 9.2 for the larger container and Fig. 5.3 for the smaller container) and decreases the heating time only marginally. Hence, from the consideration of power utilization above, the optimal power would suggest a heater flux of around 0.5 W/in<sup>2</sup>.

### 9.3 Effect of Initial Temperature

The initial temperature of the nutrient material is the most influential factor on heating time requirements. Figure 9.3 depicts the time responses for foods initially in the frozen and ambient initial states for a range of thermal diffusivity. As expected the initially frozen foods heat slowly. For nutrient materials with thermal diffusivity below that of water, the model predicts heating times over three hours to reach 140F. However, almost an hour is required to reach 45F; so that the total time in the critical range (45-140F) is not so long as it first might appear.

### 9.4 Effect of Container Size

It is desirable during the heating process to have the maximum heat transfer surface area per given volume of food. For a cylindrical container heated on the sides and bottom, this size

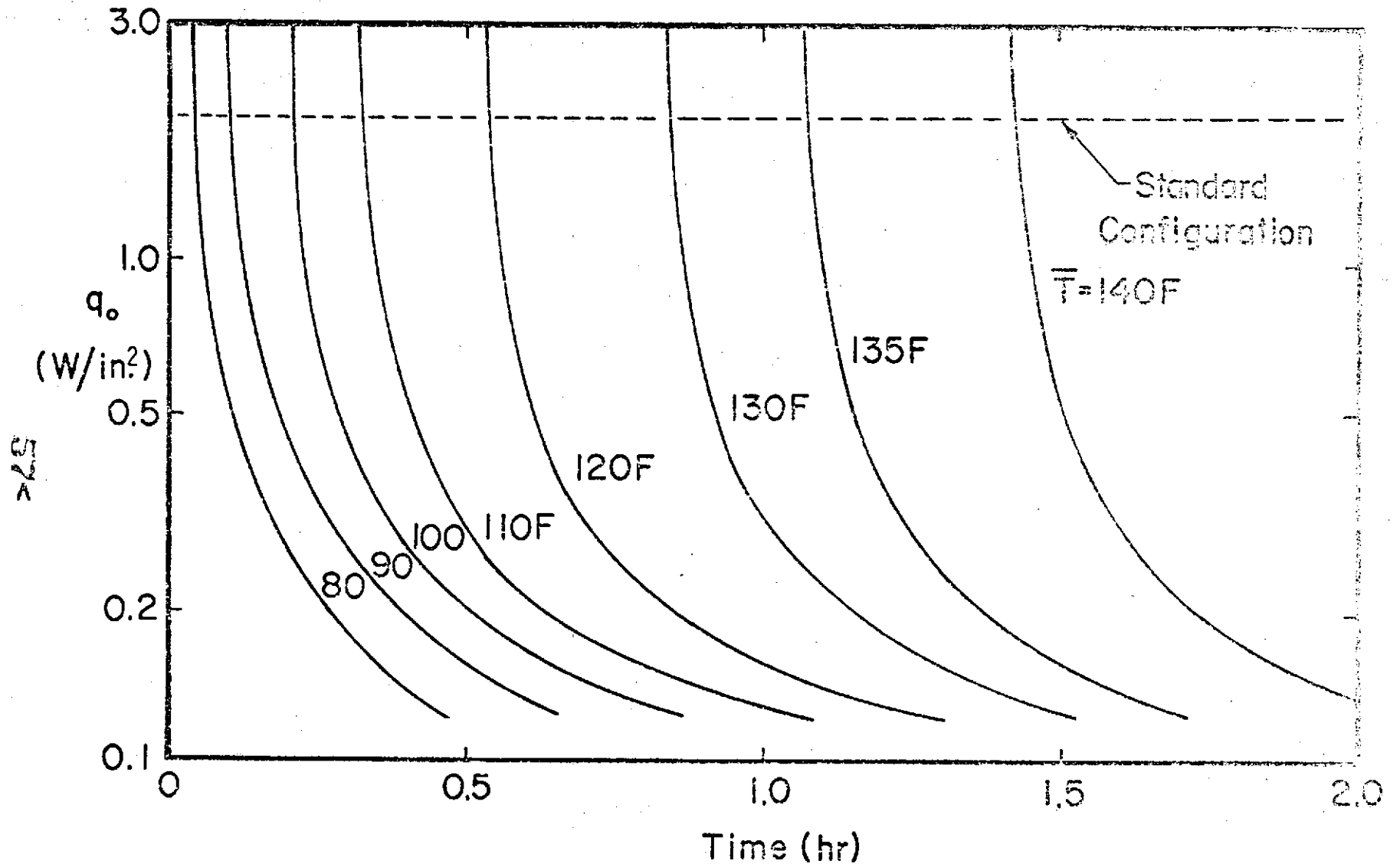
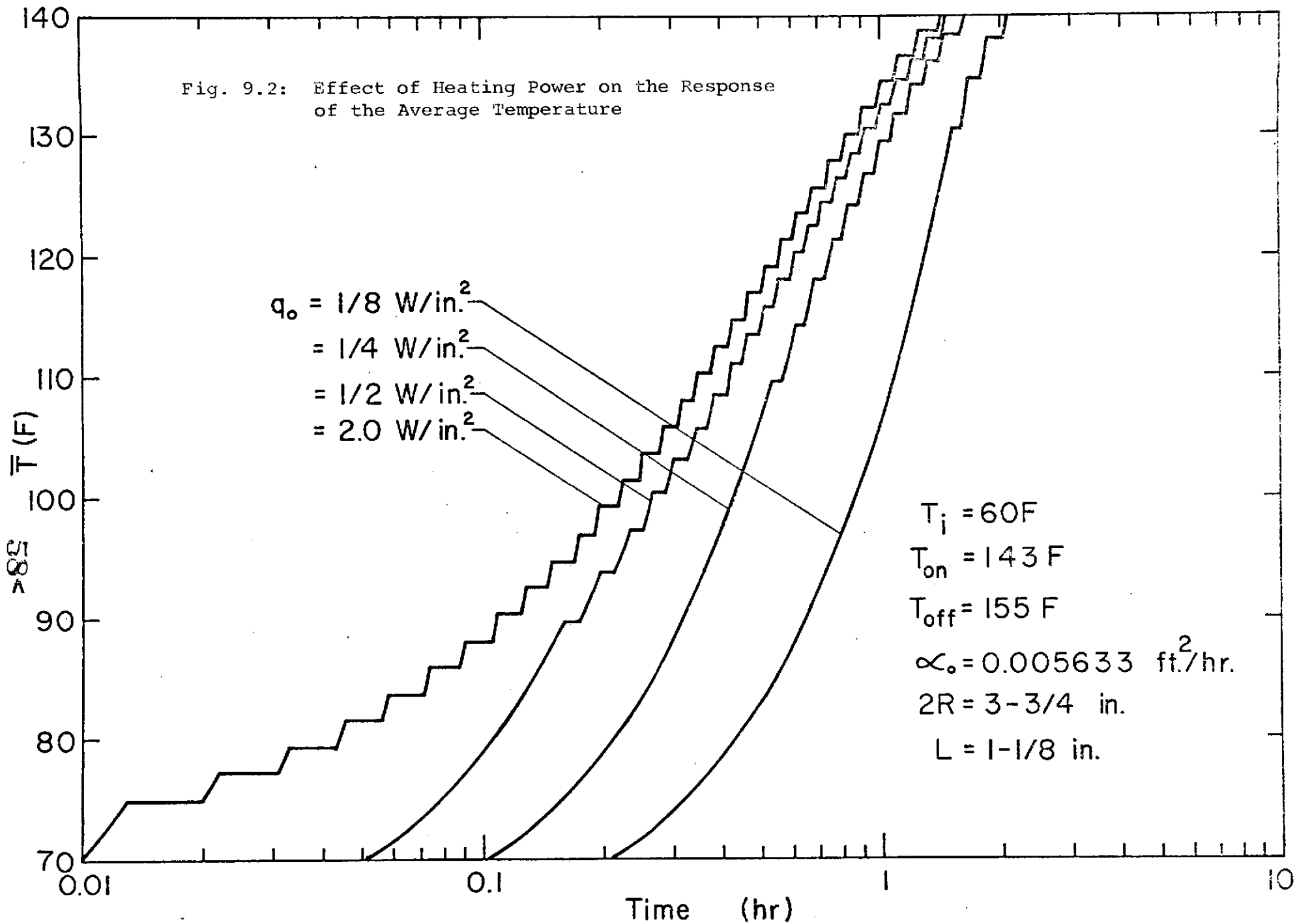


Fig 9.1: Time for the Average Temperature to Reach Various Levels as the Heater Power Level Changes for the Standard Configuration

Fig. 9.2: Effect of Heating Power on the Response of the Average Temperature



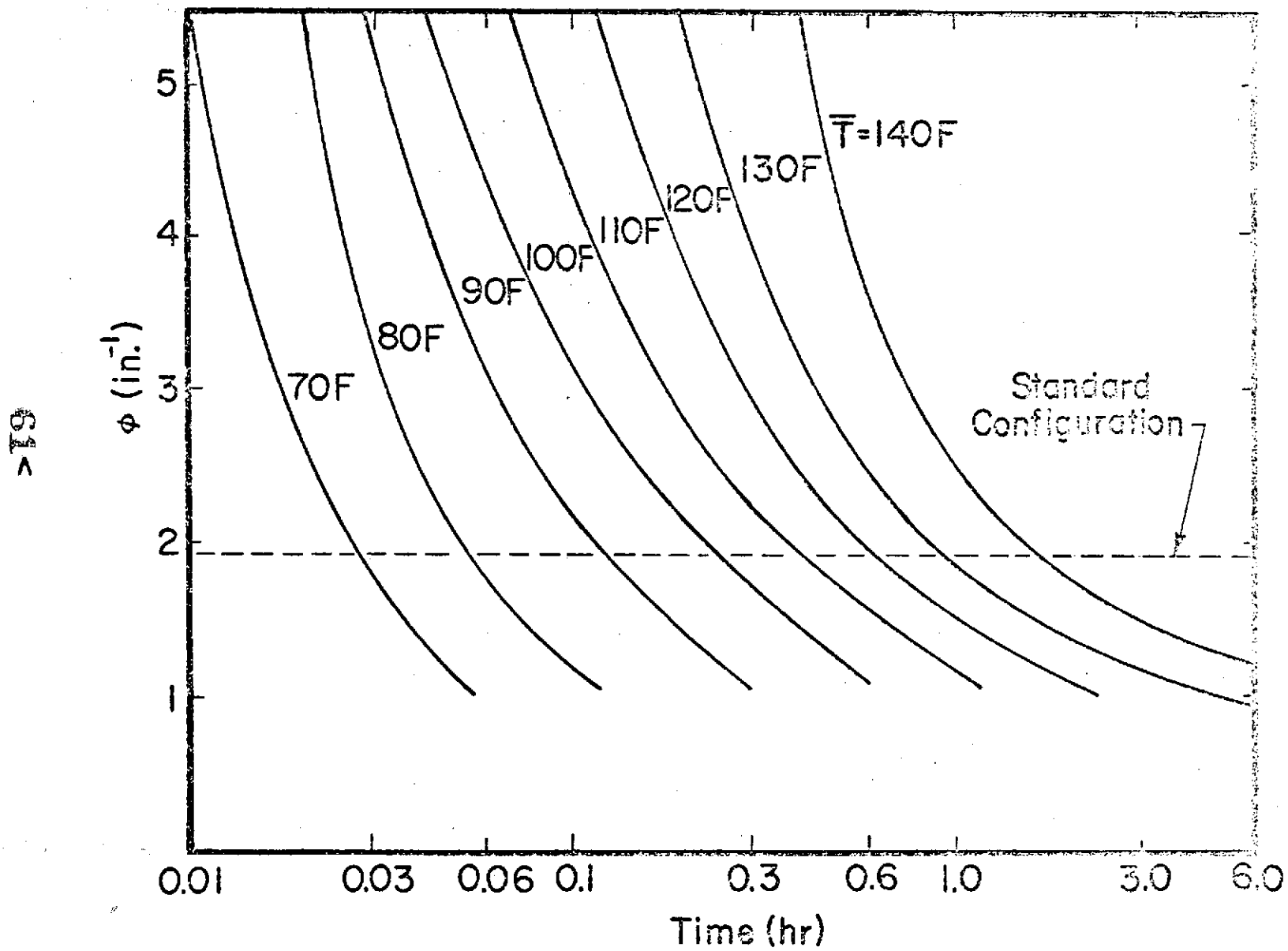


Fig. 9.4: Time for the Average Temperature to Reach Various Levels as the Size Parameter Changes for the Standard Configuration

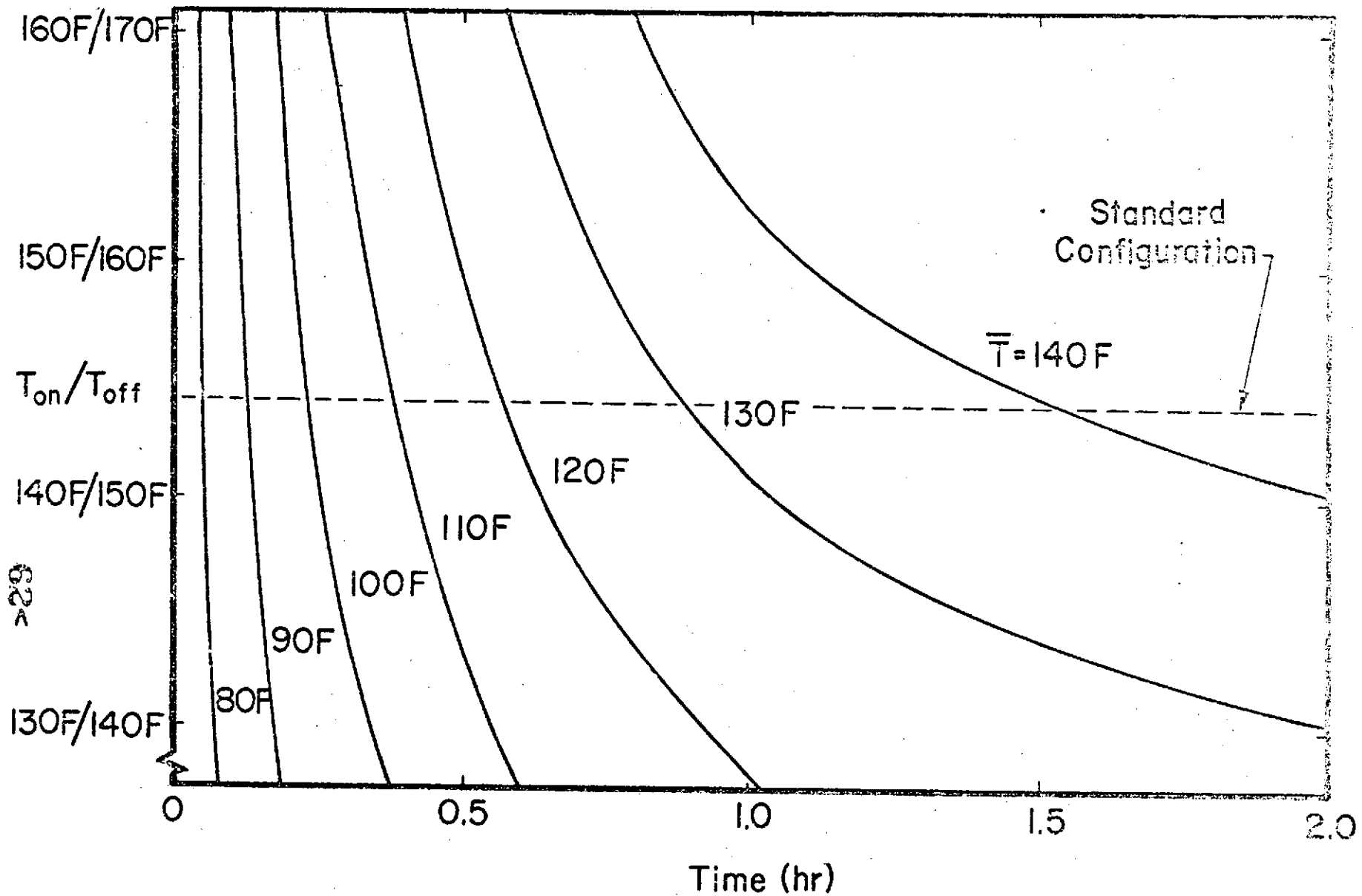


Fig. 9.5: Time for the Average Temperature to Reach Various Levels as the Heater Control Temperatures Change for the Standard Configuration

average temperature to various levels is presented as a function of  $T_{on}/T_{off}$  ratios where  $T_{off} - T_{on} = 10F$ . Of particular interest is the fact, increasing the level above 150F/160F does not decrease the heating time significantly.

#### 9.6 Discussion

In this report a thermal analysis of the proposed Skylab food heating system has been presented. A finite difference model was used to carry out parametric studies to determine the effect on heating time of (a) thermal diffusivity, (b) heater power level, (c) initial temperature (d) container size, and (e) control temperatures. A summary of the results is indicated in Fig. 9.6. These curves represent the time required for the standard configuration model to be heated to an average temperature of 140F as one of the model parameters is allowed to vary. The intersection of all the lines represents the Skylab configuration for heating water from an initial temperature of 60F. As the configuration varies the change in heating time can easily be determined by following the appropriate curve. In particular, it is noted that lowering by one-fourth the heater power level does not greatly effect the heating time.

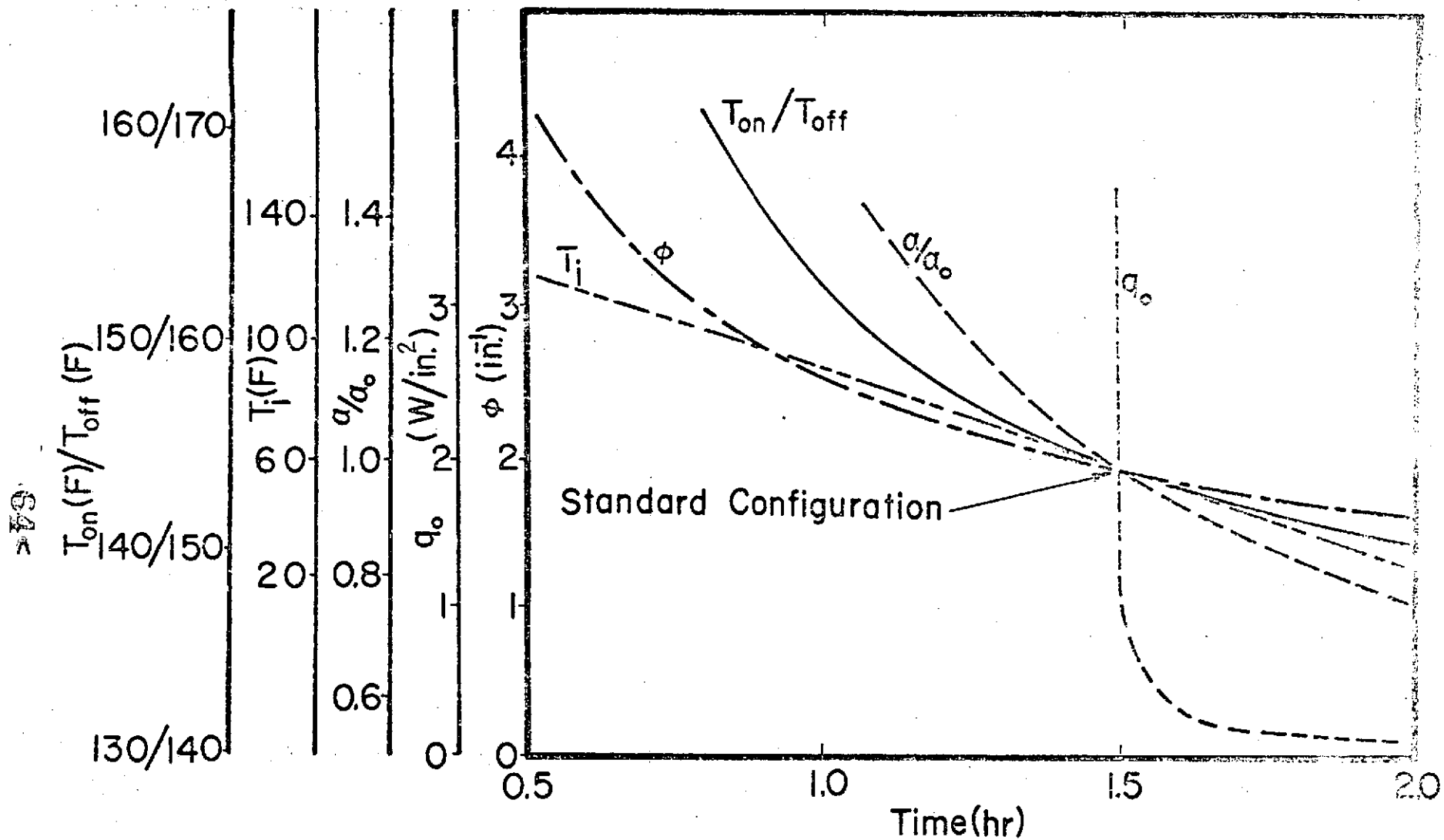


Fig. 9.6: Time for the Average Temperature to Reach 140F as Each of the Problem Parameters Vary (one at a Time) from the Standard Configuration

## REFERENCES

- [10] Earle, R. L., Unit Operations in Food Processing, Pergamon Press, New Zealand, 1966.
- [11] Elizalde, J. C., "Orbital Tests to Investigate Thermal Behavior of Cryogenes under Weightlessness," Proceedings of the Conference on Propellant Tank Pressurization and Stratification, Vol. II, NASA/MSFC, Huntsville, Alabama, January, 1965, pp. 245-280.
- [12] Otto, E. W., "Static and Dynamic Behavior of the Liquid-Vapor Interface during Weightlessness," Proceedings of the Conference on Propellant Tank Pressurization and Stratification, Vol. II, NASA/MSFC, Huntsville, Alabama, January, 1965, pp. 283-354.
- [13] Petrash, D. A., "Experimental Study of the Effects of Weightlessness on the Configuration of Mercury and Alcohol in Spherical Tanks," NASA TX-1197, April, 1962.
- [14] Tyler, B. J., "Heat Transfer to a Gas from a Spherical Enclosure: Measurements and Mechanisms," International Journal of Heat and Mass Transfer, Vol. X, Pergamon Press, 1967, pp. 251-253.
- [15] Siegel, R., "Effects of Reduced Gravity on Heat Transfer," Advances in Heat Transfer, Vol. IV, Academic Press, 1967, pp. 144-222.
- [16] Holman, J. P., Heat Transfer, McGraw-Hill Book Company, New York, 1972.
- [17] Sweat, Vincent E., "Heating of Food in Modified Atmospheres," Final Report Contract No. NAS 9-10823.